University of Sassari

Department of Biomedical Sciences

PhD School in Life Sciences and Biotechnologies

Director: Leonardo A. Sechi

Cycle XXXII

Nanotechnology applications: from bone regeneration to cancer therapy

Supervisor:

Prof. Luigi Marco Bagella

PhD Candidate:

Valentina Bordoni

Academic Year: 2018-2019

La presente tesi è stata prodotta durante la frequenza del corso di dottorato in Life Sciences and Biotechnologies dell'Università degli Studi di Sassari, A.A. 2018/2019 – XXXII ciclo, con il sostegno di una borsa di studio finanziata con le risorse del P.O.R. SARDEGNA F.S.E. 2014-2020 Asse III - Istruzione e Formazione - Obiettivo Tematico 10 "Investire nell'istruzione, nella formazione e nella formazione professionale per le competenze e l'apprendimento permanente".

1. Abstract **4**
2. Introduction **5**
2.1 Nanomedicine and its applications **5**
2.2 Nanomedicine and Bone regeneration **7**
2.2.1 Promising nanomaterials for bone regeneration **7**
2.3 Nanomedicine and Cancer **10**
2.3.1 Emerging nanoparticles in cancer medicine **10**
2.4 Reference **13**
3. Aim of the thesis **17**
4. Graphene oxide in bone regeneration **18**
4.1 Introduction **18**
4.2 Materials and methods **20**
4.2.1 Nanomaterials: synthesis and characterization **20**
4.2.2 Cell culture **20**
4.2.3 Apoptosis and viability assay **21**
4.2.4 Activation assay **22**
4.2.5 ALP and alizarin red S **22**
4.2.6 Real-time PCR and osteogenesis array **23**
4.2.7 OSM and TLR2/4 evaluation in hMSCs differentiation **23**
4.2.8 Mice **24**
4.2.9 Flow cytometric analysis of immune cells **24**
4.2.10 µCT measurement **24**
4.2.11 Bone histology **25**
4.2.12 Statistical analysis **25**
4.3 Results and discussion **26**
4.3.1 Synthesis of maGO-CaP and cell viability **26**
4.3.2 Monocytes Activation **29**
4.3.3 Osteoblast differentiation in the presence of monocytes **30**
4.3.4 maGO-CaP osteogenesis mechanisms **35**
4.3.5 Osteogenesis process mediated by maGO-CaP: the role of monocytes **38**
4.3.6 *In vivo* bone formation **42**
4.4 Conclusions **48**
4.5 Reference **50**
5. Silver nanoparticles and cancer treatment **53**
5.1 Introduction **53**
5.2 Materials and methods **55**
5.2.1 *Artemisa*-AgNPs synthesis and characterization **55**
5.2.2 Cell cultures **55**
5.2.3 Proliferation assay (XTT) **55**
5.2.4 Cell cycle analysis **56**
5.2.5 Necrosis and apoptosis evaluation **56**
5.2.6 Colony assay **56**
5.2.7 mRNA extraction and preparation of mRNA-seq library **57**
5.2.8 Quality Control and Gene Analysis **57**
5.2.9 GO Enrichment and KEGG Pathway Analysis **58**
5.2.10 Key modules and hub genes identification **59**
5.3 Results and discussion **60**
5.3.1 Synthesis and cytotoxic effects of *Artemisia*-AgNPs on cancer cell lines **60**
5.3.2 Cell cycle impact **64**
5.3.3 *Artemisia*-AgNPs induce apoptosis and inhibit colony formation in cancer cells **66**

5.3.4 *Artemisia*-AgNPs impact on gene expression **68**
5.4 Conclusions **75**
5.5 Reference **76**
6. Conclusions and future perspective **78**

1. Abstract

Nanotechnology is still one of the best promises to overcome the major challenges of modern medicine. In this work, we identified innovative nanotools as potential candidates in two main biomedical applications: bone regeneration and cancer treatment.

Knowing the strict correlation between the immune system function and the bone regeneration, nanomaterials able to combine and sustain an immune-mediated bone renewal are still missing. Considering the promising use of graphene, we exploited the intrinsic immune-characteristics of a specific Graphene Oxide (GO) and the well-known osteoinductive capacity of Calcium Phosphates (CaP) in a novel unique biocompatible nanomaterial called maGO-CaP (Monocytes Activator Graphene Oxide conjugated with Calcium Phosphates). This new material demonstrates, by performing *in vitro* and *in vivo* analysis, its ability to induce osteoinductive stimuli capable to increase bone regeneration.

A very important challenge in medical research is the fight against cancer. In this context, silver nanoparticles (AgNPs) represent a promising nano-tool able to offer an interesting option for cancer therapy. We proposed a "green" synthesis method to produce AgNPs, using *Artemisia arborescens* extracts. We investigated the potential antiproliferative and anticancer proprieties of *Artemisia*-AgNPs using several approaches, from cell cycle analysis to RNA-sequencing, demonstrating the potentiality of *Artemisia*-AgNPs as a suitable candidate agent in cancer research.

2. Introduction

Nanotechnology is a scientific discipline that requires a multidisciplinary approach leading to the development of nanocomposites for several applications, including biology and medicine. The nanotechnological procedures involve the design, characterization and application of nanostructures by monitoring the physicochemical properties. [1] The term "nano" is used to indicate the matter with at least one dimension sized from 1 to 100 nanometers. Nanomaterials and nanoparticles show a high ratio between surface area and volume and they can be functionalized with a wide variety of compounds. These characteristics make them excellent candidates for biomedical applications. Indeed, nanomedicine represents an emerging research field of nanotechnology, with the aim to synthesize nano-objects for therapeutic and diagnostic purposes. Nanomedicine is based on the development of nano-systems for medical applications as potential tools for diagnosis and therapy, biological devices and biosensors. [2] This new scientific discipline is intended to provide action at a molecular level, in order to overcome traditional therapies and improve the efficacy of treatments on the road to a more personalized medicine. [3]

2.1 Nanomedicine and its applications

Engineer nanoparticles and nanomaterials are the key components of nanomedicine and, currently, a large variety of nanoparticle types exist, just some examples are: lipid micelles, carbon nanotubes (CNTs), graphene, nanodiamonds, superparamagnetic iron oxide nanoparticles (SPIONs), magnetic nanoparticles, silver, gold and silica nanoparticles and more.

Applications of nanomedicine are especially promising and are focusing on different medical areas such as pharmacological, therapy, diagnostics and imaging, but also prostheses, implants and medical devices. **Scheme 1** summarizes the main nano-compounds investigated for their potential applications in nanomedicine.

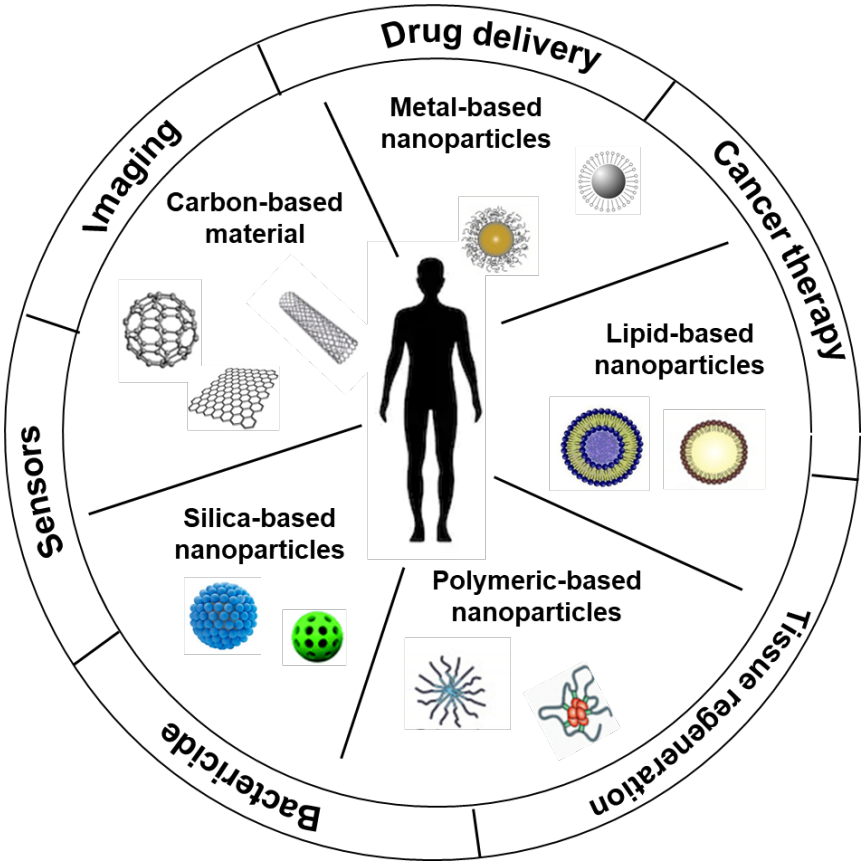

Scheme 1. Nanomedicine applications

Nanomedicine provides the possibility of delivering drugs to specific cells using nanoparticles with the purpose i) to improve drug stability, ii) to reduce adverse drug side effects, iii) to maximize the bioavailability of medications at specific places in the body and iv) to improve their efficacy regulating the drug release. [4, 5]

The combination of drug delivery and multi-modality treatment with therapeutic and diagnostic approaches is defined as “theranostic”. The theranostic nanoparticle is a unique system, which at the same time enables diagnosis, therapy, and monitoring of therapeutic response. [6] Nanoparticles can be functionalized with several ligands with therapeutic effect or ability to direct nanoparticle fate and monitoring the system. [7, 8]

Nanomedicine can be applied also in tissue engineering to reproduce or repair damaged tissues. Suitable nanomaterial-based scaffolds have been engineered to enhance cell adhesion, proliferation, differentiation as well as promoting tissue growth. Scaffolds can be designed with specific biochemical, mechanical and electrical characteristics to mimic the native tissues.

Nanomedicine offers the potential to revolutionize almost all branches of medicine and to pave the way for an improvement of treatment efficacies and more personalized medicine. Nevertheless, the optimization and the complete understanding of the potential and limitations of nanoparticulate systems require additional studies and research.

2.2 Nanomedicine and Bone regeneration

The treatment of systemic bone diseases and the management of bone fractures is a crucial point in medical research as the incidence of bone disease, such as osteoporosis, is constantly increasing. [9] The challenging goal of science in regenerative medicine is to find a way to promote bone formation and to maintain homeostasis of this tissue to improve bone health and quality of life in affected patients. Bone tissue engineering is based on the recruitment of osteoprogenitor cells and the stimulation of their proliferation and differentiation, inducing remodeling of the bone. [10] Nanotherapeutic strategies in bone tissue engineering have seen recent progress on several fronts. Nanoparticles may be employed for osteogenic drugs, growth factors and gene delivery, or may be incorporated into scaffolds to enhance mechanical stability, biocompatibility, and cell survival for implanted constructs. [11] Moreover, nanoscale features result in osteogenic effects, acting over multiple aspects of mesenchymal stem cells and osteoblast behavior, including adhesion, migration, proliferation, gene expression and stem cell fate. [12]

2.2.1 Promising nanomaterials for bone regeneration

The ability to mimic hierarchical and nanoscale structures of bone, the high ratio between strength and weight, the capacity to deliver growth factors and drugs and the tissue regeneration potential make nano-systems promising tools in orthopedic applications. [13] Recently, scaffolds manufactured from nanofibers, nanotubes, nanoparticles and hydrogel have been studied to replace efficiently the defective tissues. In **Table 1,** various nanomaterials currently investigated in the bone regeneration process are summarized.

Nanomaterials	Characteristics and medical applications	References
Nanosilicates	• inorganic nanomaterials • biocompatible • drug delivery • bone regeneration	[14, 15]
Nanohydroxyapatite	• component of enamel • increase bioactivity of hydroxyapatite • bone regeneration	[16]
Carbon nanotubes	• tensile strength • thermal conductivity • electrical conductivity • drug delivery • nanotechnology engineering • tissue regeneration	[17, 18, 19]
Graphene	• thermally conductive • mechanical strength • high elasticity • biological engineering • drug delivery • antimicrobial applications • tissue regeneration	[20, 21, 22]

Table 1. Nanomaterials and bone regeneration.

a) *Nanosilicates*

Nanosilicates are bioactive inorganic nanomaterials composed of hydrous sodium lithium magnesium silicate, which are currently found to be safe and effective for bone formation. Magnesium ions play an important role in cellular adhesion of osteoblasts, stimulating the interaction of gap junctions and integrin family proteins. [23, 24] Moreover, lithium can suppress the activity of GSK-3β, stimulating the Wnt-signaling pathway, which is involved in osteogenesis mechanism. [25] Thanks to the high surface-to-volume ratio and charged surface, nanosilicates can be conjugated with several compounds and can modulate the release of multifunctional molecules. [26] Several studies reported the effects of laponite-nanosilicates being able to control the release of drugs and growth factors, becoming an interesting material for bone induction. [26, 27]

b) *Nanohydroxyapatite*

Hydroxyapatite (HAP) is the main component of enamel and it is also an important resource of calcium and phosphate, essential for the remineralization process. The nano-size of hydroxyapatite

(nHAP) increases the surface area to which specific proteins bind and enhances the bioactivity of hydroxyapatite. [28] nHAP is able to promote protein adhesion, cell proliferation and integration, becoming a popular bone substitute. Several studies demonstrated the properties of nHAP to enhance bone formation, stimulating bone growth and development. [29, 30, 31]

c) *Carbon nanotubes*

Carbon nanotubes (CNTs) are tubes made of carbon, with a nanoscale diameter. Carbon nanotubes can be single-wall carbon nanotubes (SWCNTs) or multi-wall carbon nanotubes (MWCNTs) consisting of nested single-wall carbon nanotubes. SWCNTs are different from MWCNTs for diameter range and length. CNTs own interesting properties, such as exceptional tensile strength and thermal and electrical conductivity. They have been investigated for several biomedical applications, including tissue engineering, [18] imaging, [32] biosensors [33] and drug delivery. [17] The choice of size, length and surface modification of CNTs determines the achievement of specific characteristics effective for bone growth. [34] CNTs can be combined, for example, with hydroxyapatite to enhance bone regeneration. [35]

d) *Graphene*

Graphene is a two-dimensional allotrope of carbon, where the atoms are binding together in a hexagonal lattice. It is the basic structural element of other carbon-based materials such as carbon nanotubes and fullerenes. It shows promising physicochemical proprieties for many applications, [36] including a highly thermally conductive [37] and superior mechanical strength (one hundred times more than steel) and, at the same time, high elasticity. [38] Moreover, graphene has well-established surface chemistry, [39] with a large surface area, which can be multifunctionalized with several chemical compounds, including drugs or specific targeting molecules. [40] Thanks to these distinctive physicochemical characteristics, the applications of graphene and its derivatives are growing in medical research. [41] In particular, recent evidences suggest a potential use of graphene-based materials in stimulating bone formation. [42] Graphene oxide has positive effects on cell adhesion, proliferation and differentiation, stimulating osteogenic differentiation. Moreover, graphene oxide can be conjugated with calcium phosphate to obtain greatest performance in the bone regeneration field, giving a synergistic acceleration in the osteogenesis, without any toxicity. [43]

2.3 Nanomedicine and Cancer

One of the most important nanomedicine applications is related to the world of oncology and cancer therapy. The treatment of cancer, up to date, is based on surgery, radiation, and chemotherapy. The main risks correlated to all these therapies are the damage of normal tissue and the incomplete eradication of the tumor. In this context, nanotechnology may offer the opportunity to fight cancer reducing toxicity on healthy cells, improving pharmacokinetic and pharmacodynamic profiles of existing anticancer compounds and combining cancer therapies. [44, 45] Moreover, nanosystems can be useful to provide more sensitive cancer detection by the development of a biosensor to identify tumor biomarkers or precancerous cells. [46] Nanoparticles and nanomaterials have become subjects of fundamental research as possible effective platforms for diagnosis and therapeutic outcome. The design of nanoparticles is essential to define their behavior. The features of nanoparticles, including size, shape, charge, coating, cargo, and material, influence their ability to move and interact with the environment and cells. [47] Moreover, the surface of nanoparticles can be functionalized and manipulated by conjugating functional molecules, including therapeutic agents, fluorescent dye and targeting ligands. [48, 49] In other words, it is possible to target therapies directly and selectively to cancerous cells, to guide in surgical resection of tumors and to improve the therapeutic efficacy, decreasing adverse side-effects.

2.3.1 Emerging nanoparticles in cancer medicine

Nowadays, a wide variety of nanoparticles have been studied for the development of cancer nanomedicines. [50, 51, 52] **Table 2** shows some of the major nanoparticles with potential applications in cancer as drug delivery systems, imaging tools and possible therapeutic agents.

Nanomaterials	Characteristics	Potential use in cancer	Reference
Liposome	• spherical vesicles • made of phospholipids • biocompatibility • biodegradability • low toxicity	nano-carriers for anticancer drugs	[53, 54]
Superparamagnetic Iron-Oxide Nanoparticles	• spherical particle • diameter 1-100nm • magnetic properties • biocompatible	• drug delivery • cancer magnetic nanotherapy • tumor targeting • medical imaging	[55, 56]
Silver nanoparticles	• size 1-100 nm • spherical, diamond, octagonal, sheets	• potential carriers for anticancer drugs • potential anticancer agents	[57,58]

Table 2. Promising nanoparticles for cancer therapy.

I) Liposome

Liposomes are spherical vesicles, described for the first time by Bangham in 1961. [59] Liposomes consist mainly of phospholipids, especially phosphatidylcholine, but may also contain other lipids. Liposomes may incorporate a small amount of molecules and surface ligands to achieve site-specific. [60, 61] Thanks to this aptitude to embed hydrophilic and lipophilic drugs plus the high biocompatibility, biodegradability and low toxicity, [62] liposomes have been investigated, in the last years, in cancer therapy as drug delivery system, able to decrease drug toxicity, to protect chemotherapeutic agents from the surrounding environment and to target the desired site of action. Up to date, there are several liposomal-based nano-carriers incorporating anticancer drugs, such as doxorubicin and daunorubicin, approved by the FDA or used in clinical trials as potent anticancer formulations. [63, 64] In summary, liposomes can be considered attractive vehicles for targeted delivery of anticancer agents.

II) Superparamagnetic Iron-Oxide Nanoparticles

Superparamagnetic Iron-Oxide Nanoparticles (SPIONs) are particles with a diameter range between one and 100 nanometers. SPIONs, such as magnetite (Fe_3O_4) and maghemite (Fe_2O_3), show unique physical, chemical, magnetic and biocompatibility properties. By exploiting magnetic force, SPIONs have been successfully used for target drug delivery. [65, 66] SPIONs reveal superparamagnetic effects when they are reduced to 10–20 nm, determining magnetization until their saturation, without any

residual magnetism after magnetic field termination. [67] Through a high-gradient magnetic field is possible to concentrate SPIONs at a specific target site of tissue. [68] Moreover, SPIONs, thanks to superparamagnetic proprieties and easy surface modification, have been extensively investigated as contrast agents in magnetic resonance imaging (MRI). [69] SPIONs are interesting nanoparticles for cancer research thanks to their ability to combine cancer magnetic nanotherapy, tumor targeting and medical imaging in theranostic approach. [70, 71, 72]

III) Silver nanoparticles

Silver nanoparticles are nanoparticles made of metallic silver of between 1 nm and 100 nm in size. The shape of these nanoparticles depends on the synthetic method used to prepare them and determine the field of application according to their specific properties. Usually, silver nanoparticles are spherical but diamond, octagonal and thin sheets are also common. Silver is a strong bactericidal agent [73] and it has been demonstrated that *in vitro* several silver complexes showed active effects against cancer. [74] By exploiting the anti-cancer properties of silver and improving its bioavailability, silver nanoparticles (AgNPs) represent a promising nano-tool able to offer an interesting implement for many biomedical applications. The extremely large surface area of silver nanoparticles offers the possibility to conjugate them with a wide variety of ligands. [75] Therefore, silver nanoparticles have been investigated as potential carriers for delivering various biomolecules or small drugs, including anticancer molecules, to specific targets. [76, 77] Once the nanoparticles reach their target, following internal or external stimulus, they can release chemotherapeutic agents at specific sites minimizing side effects. [78] Moreover, several studies demonstrated the antiproliferative and apoptosis-inducing proprieties of silver nanoparticles, proposing them as potential anticancer agents. [79, 80]

2.4 Reference

[1] T. Appenzeller, *Science,* **1991**, 254, 1300.

[2] V. Dusastre, *Nature*, **2008**, 451, 770.

[3] K.K. Wong, X.L. Liu, *Pediatr Surg Int*, **2012**, 10, 943.

[4] R. Ranganathan, S. Madanmohan, A. Kesavan, G. Baskar, Y. R Krishnamoorthy, R. Santosham, D. Ponraju, S. K. Rayala, G. Venkatraman, *International Journal of Nanomedicine*, **2012**, 7, 1043.

[5] T.M. Allen, P.R. Cullis, *Science*, **2004**, 303, 1818.

[6] J.H. Ryu, H. Koo, I.C. Sun, S.H. Yuk, K. Choi, K. Kim, I.C. Kwon, *Adv Drug Deliv Rev*, **2012**, 13, 1447.

[7] L. Zhang, S.R. Jean, S. Ahmed, P.M. Aldridge, X. Li, F. Fan, E.H. Sargent, S.O. Kelley, *Nat Commun*, **2017**, 1, 381.

[8] J. Cao, R. Ge, M. Zhang, J. Xia, S. Han, W. Lu, Y. Liang, T. Zhang, Y. Sun, *Nanoscale*, **2018**, 10, 9021.

[9] N.B. Watts, J.E. Manson, *Jama*, **2017**, 317, 253.

[10] P.V. Giannoudis, H. Dinopoulos, E. Tsiridis, *Injury*, **2005**, 36, S20.

[11] G.G. Walmsley, A. McArdle, R. Tevlin, A. Momeni, D. Atashroo, M.S. Hu, A.H. Feroze, V.W. Wong, P.H. Lorenz, M.T. Longaker, D.C. Wan, *Nanomedicine*, **2015**, 11, 1253.

[12] T. Gong, X. Jing, L. Jinfeng, T. Zhang, L. Shiyu, L. Yunfeng, *Bone Research*, **2015**, 3, 15029.

[13] L. Zhang, T.J. Webster, Nano today, **2009**, 4, 66.

[14] Y. Wang, W. Cui, J. Chou, S. Wen, Y. Sun, H. Zhang, *Colloids Surf B Biointerfaces*, **2018**, 172, 90.

[15] M. Jain, K. Matsumura, *J Biomed Mater Res A,* **2016**, 104, 1379.

[16] H. Wang, Y. Li, Y. Zuo, J. Li, S. Ma, L. Cheng, *Biomaterials*, **2007**, 28, 3338.

[17] A. Bianco, K. Kostarelos, M. Prato, *Current Opinion in Chemical Biology*, **2005**, 9, 674.

[18] S. Bosi, L. Ballerini, M. Prato, *Top Curr Chem*, **2014**, 348, 181.

[19] P. Newman, A. Minett, R. Ellis-Behnke, H. Zreiqat, *Nanomedicine*, **2013**, 9, 1139.

[20] P. Kumar, P. Huo, R. Zhang, B. Liu, *Nanomaterials*, **2019**, 9, 737.

[21] S. Goenka, V. Sant, S. Sant, *J Control Release*, **2014**, 173, 75.

[22] N. Shadjou, M. Hasanzadeh, B. Khalilzadeh, *Bioengineered*, **2018**, 9, 38.

[23] L.Y. He, X.M. Zhang, B. Liu, Y. Tian, W.H. Ma, *Braz J Med Biol Res*, **2016**, 49, e5257.

[24] H. Zreiqat, C. Howlett, A. Zannettino, P. Evans, G. Schulze-Tanzil, C. Knabe, M. Shakibaei, *Journal of Biomedical Materials Research*, **2002**, 62, 175.

[25] L. Li, P. Xiaozhong, Q. Yongbao, W. Renchong, T. Jingli, C. Xu, W. Ting, L. Wenlong, P. Haobo, L. Bing. *Scientific Reports*, **2017**, 7, 45204.

[26] J. Min, R.D. Braatz, P.T. Hammond, *Biomaterials*, **2014**, 35, 2507.

[27] J.I. Dawson, J.M. Kanczler, X.B. Yang, G.S. Attard, R.O. Oreffo, *Advanced materials*, **2011**, 23, 3304.

[28] H. Zhou, J. Lee, *Acta Biomater,* **2011**, 7, 2769.

[29] S. Tavakol, M. Nikpour, A. Amani, M. Soltani, S. Rabiee, *Journal of nanoparticle research*, **2013**, 15, 1373.

[30] A.K. Teotia, D.B. Raina, C. Singh, N. Sinha, Isaksson H, M. Tägil, L. Lidgren, A. Kumar, *ACS Applied Materials & Interfaces*, **2017**, 9, 6816.

[31] P. Kubasiewicz-Ross, J. Hadzik, J. Seeliger, K. Kozak, K. Jurczyszyn, *Annals of Anatomy-Anatomischer Anzeiger*. **2017**, 213, 83.

[32] L.G. Delogu, G. Vidili, E. Venturelli, C. Menard-Moyon, M.A. Zoroddu, G. Pilo, P. Nicolussi, C. Ligios, D. Bedognetti, F. Sgarrella, R. Manetti, A. Bianco, *Proc Natl Acad Sci U S A*, **2012**, 109, 16612.

[33] R.J. Chen, S. Bangsaruntip, K.A. Drouvalakis, N.W. Kam, M. Shim, Y. Li, W. Kim, P.J. Utz, H. Dai, *Proc Natl Acad Sci U S A*, **2003**, 100, 4984.

[34] E. Hirata, *J. Dent. Sci*, **2017**, 99, 103, 2017.

[35] S. Mukherjee, S.K. Nandi, B. Kundu, A. Chanda, S. Sen, P.K. Das, *J Mech Behav Biomed Mater,* **2016***,* 60, 243.

[36] A.K. Geim, K.S. Novoselov, *Nat Mater*, **2007**, 6, 183.

[37] G. Xin, T. Yao, H. Sun, S.M. Scott, D. Shao, G. Wang, J. Lian, *Science*, **2015**, 349, 1083.

[38] A.K. Geim, K.S. Novoselov, *Nat Mater.*, **2007**, 6, 183.

[39] H. Jiang, *Small*, **2011**, 7, 2413.

[40] M. Orecchioni, C. Menard-Moyon, L.G. Delogu, A. Bianco, *Adv Drug Deliv Rev*, **2016**, 105, 163.

[41] M. Orecchioni, R. Cabizza, A. Bianco, L.G. Delogu, *Theranostics*, **2015**, 5, 710.

[42] N. Dubey, R. Bentini, I. Islam, T. Cao, A. Helio, C. Neto, V. Rosa1*, Stem cells international,* **2015**, 2015, 804213.

[43] R. Tatavarty, H. Ding, G. Lu, R.J. Taylor, X. Bi, *Chemical communications*, **2014**, 50, 8484.

[44] A. Wicki, D. Witzigmann, V. Balasubramanian, J. Huwyler, *J. Control. Rel.,* **2015**, 200, 138.

[45] E. Blanco, A. Hsiao, A.P. Mann, M.G. Landry, F. Meric-Bernstam, M. Ferrari, *Cancer Sci*., **2011**, 102, 1247.

[46] A. Gdowski, A.P. Ranjan, A. Mukerjee, J.K. Vishwanatha, *Adv Exp Med Biol.*, **2014**, 807, 33.

[47] S. Hauert, S.N. Bhatia, *Trends Biotechnol*., **2014**, 32, 448.

[48] J.D. Byrne, T. Betancourt, L. Brannon-Peppas, *Adv. Drug Deliv.Rev.*, **2008**, 60, 1615.

[49] N.R. Jabir, S. Tabrez, G.M. Ashraf, S. Shakil, G.A. Damanhouri, M.A. Kamal, *Int. J. Nanomed.* **2012**, 7, 4391.

[50] M. Ferrari, *Nat. Rev. Cancer*, **2005**, 5, 161.

[51] H. Havel, G. Finch, P. Strode, M. Wolfgang, S. Zale, I. Bobe, H. Youssoufian, M. Peterson, M. Liu, *AAPS J.*, **2016**, 18, 1373.

[52] R. Tong, D.S. Kohane, *Annu. Rev. Pharmacol. Toxicol.*, **2016**, 56, 41.

[53] T. Olusanya, R. R. Haj Ahmad, D. M. Ibegbu, J. R. Smith, A. A. Elkordy, *Molecules*, **2018**, 23, 907.

[54] S. Hossen, M. K. Hossain, M.K. Basher, M. Mia, M.T. Rahman, M. J. Uddin, *Journal of advanced research*, **2018**, 15, 1.

[55] C. Janko, T. Ratschker, K. Nguyen, L. Zschiesche, R. Tietze, S. Lyer, C. Alexiou, *Frontiers in oncology,* **2019**, 9, 59.

[56] J. Dulinska-Litewka, A. Łazarczyk, P. Hałubiec, O. Szafranski, K. Karnas, A. Karewicz, *Materials*, **2019**, 12, 617.

[57] S.J.D.S. Doddapaneni, C. Amgoth, A.M. Kalle, S.N. Suryadevara, K.S. Alapati, *3 Biotech*, **2018**, 8, 156.

[58] M.A. Ebrahimzadeh, A. Tafazoli, J. Akhtari, P. Biparva, S. Eslami, *Anticancer Agents Med Chem,* **2018**, 18, 1962.

[59] A.D. Bangham, R.W. *Journal of Molecular Biology*, **1964**, 8, 660.

[60] V. Torchilin, *Advanced Drug Delivery Reviews*, **2006**, 58, 1532.

[61] A. Akbarzadeh, R. Rezaei-Sadabady, S. Davaran, S. Woo Joo, N. Zarghami, Y. Hanifehpour, M. Samiei, M. Kouhi, K. Nejati-Koshki, *Nanoscale Res Lett*, **2013**, 8, 102.

[62] M. Johnston, S.C. Semple, S.K. Klimuk, S. Ansell, N. Maurer, P.R. Cullis, *Biochim Biophys Acta*, **2007**, 1768, 1121.

[63] P.S. Gill, J. Wernz, D.T. Scadden, P. Cohen, G.M. Mukwaya, J.H. von Roenn, M. Jacobs, S. Kempin, I. Silverberg, G. Gonzales, M.U. Rarick, A.M. Myers, F. Shepherd, C. Sawka, M.C. Pike, M.E. Ross, *J. Clin. Oncol*., **1996**, 14, 2353.

[64] C.M. Dawidczyk, C. Kim, J.H. Park, L.M. Russell, K.H. Lee, M.G. Pomper, P.C. Searson, *J. Control Release*, **2014**, 187, 133.

[65] F.M. Kievit, M. Zhang, *Acc Chem Res*., **2011**, 44, 853.

[66] Wahajuddin, S. Arora, *Int J Nanomedicine*, **2012**, 7, 3445.

[67] D. Lombardo, M.A. Kiselev, M.T. Caccamo, *Journal of Nanomaterials*, **2019**, 2019, 26.

[68] P.B. Santhosh, N.P. Ulrih, *Cancer Letters*, **2013**, 336, 8.

[69] Z.R. Stephen, F.M. Kievit, M. Zhang, *Mater Today (Kidlington)*, **2011**, 14, 330.

[70] V.E. Orel, M. Tselepi, T. Mitrelias, A. Rykhalskyi, A. Romanov, V. Orel, A. Shevchenko, A. Burlaka, S. Lukin, *Nanomedicine: Nanotechnology, Biology and Medicine*, **2018**, 14, 1249.

[71] V. Orel, A. Shevchenko, A. Romanov, M. Tselepi, T. Mitrelias, C.H.W. Barnes, A. Burlaka, S. Lukin, I. Shchepotin, *Nanomedicine Nanotechnology Biology and Medicine*, **2015**, 11, 47.

[72] V. Orel, T. Mitrelias, M. Tselepi, T. Golovko, O. Dynnyk, N. Nikolov, A. Romanov, A. Rykhalskiy, C. Barnes, O. Yaroshenko, I. Orel, *J. Nanopharmaceutics and Drug Delivery*, **2014**, 11, 47.

[73] S. Medici, M. Peana, V.M. Nurchi, M.A. Zoroddu, *J Med Chem*., **2019**. [Epub ahead of print]]

[74] S. Medici, M. Peana, G. Crisponi, V.M. Nurchi, J.I. Lachowicz, M. Remelli, M.A. Zoroddu, *Coordination Chemistry Reviews*, **2016**, 327, 349.

[75] N. Ivanova, V. Gugleva, M. Dobreva, I. Pehlivanov, S. Stefanov, V.Andonova, *Silver Nanoparticles as Multi-Functional Drug Delivery Systems*, **2018**, book

[76] B. Buszewski, K. Rafinska, P. Pomastowski, J. Walczak, A. Rogowska, *Colloids and Surfaces A: Physicochemical and Engineering Aspects*, **2016**, 506, 170.

[77] A. Kaur, D. Goyal, R. Kumar, *Applied Surface Science*, **2018**, 449, 23.

[78] S. Mukherjee, D. Chowdhury, R. Kotcherlakota, S. Parta, B. Vinothkumar; M.P. Bhadra, B. Sreedhar, C.R. Patra, *Theranostics*, **2014**, 4, 316.

[79] A. Hekmat, A.A. Saboury, A. Divsalar, *Journal of Biomedical Nanotechnology*, **2015**, 8, 968.

[80] A. Dziedzic, R. Kubina, R.J. Bułdak, M. Skonieczna, K. Cholewa, *Molecules*, **2016**, 21, 365.

3. Aim of the thesis

Despite significant progress in medicine and biology, the research of new treatments to cure and prevent diseases and to promote regeneration of damaged tissue is still a great challenge for the scientific community. As discussed in the introduction section, nanotechnology can be considered a promising approach for the development of innovative tools in medicine. The intention of this work is to provide new insights for future applications of nanotechnology in two key research fields: bone regeneration and cancer therapy.

Considering the key role of osteoimmunology in bone regenerative medicine, materials able to interact with both immune and skeletal cells to promote bone regeneration are still missing. Depending on design and surface functionalization, graphene-based materials can be selected for exerting specific effects on the immune system. Moreover, graphene, in particular, graphene oxide, could play an important role to promote cell adhesion, proliferation and differentiation, enhancing the osteogenic differentiation for bone regeneration research. Hence the investigation of graphene oxide conjugated with calcium phosphate, which owns well-known osteoinductive properties, becomes of great interest. For the purpose of emphasizing the importance of the immune-mediated bone formation, this nanomaterial can offer real medical strategies to fight bone-related disorders.

Regarding cancer research, in the past few years, several nano-compounds have been investigated. Among them, silver nanoparticles (AgNPs) are emerging as promising nano-tools able to offer an interesting option in cancer therapy. Several studies demonstrated the potential anticancer properties of AgNPs. However, the results available on the biological responses of AgNPs are still limited. It is, therefore, crucial to have a broader overview on the impact of AgNPs, specifically those synthesized by the “green” synthesis approach, on cancer cells.

The present thesis aims to illustrate and promote the wide opportunities of nanotechnology in biomedicine fields, underlining the specific potentiality for each nano-object.

4. Graphene oxide in bone regeneration

4.1 Introduction

The development of new strategies to promote the regeneration of damaged tissues is one of the main challenges in today's regenerative medicine. [1, 2] Nanomedicine is emerging as a potential tool for bone tissue engineering, which has made huge advances in the last few years. Recent evidence shows that graphene and its derivatives, due to their unique physicochemical characteristics, distinctive nanostructure and mechanical proprieties, facilitates osteogenesis differentiation of MSCs and enhances bone regeneration. [3] In particular, graphene oxide microflakes, that were associated with ultrathin plate-shaped calcium phosphate nanoparticles (GO-CaP), were able to promote the proliferation and differentiation of human MSCs (hMSCs) *in vitro* without showing any toxicity. [4] In most studies, research on graphene in bone regeneration focused mainly on osteoblasts. [5, 6, 7] Osteoblasts arise from MSCs and their differentiation is promoted by two key pathways: the Wnt signaling pathway and the bone morphogenetic protein (BMP) pathway. Activation of both pathways leads to the stimulation of osteoblastic transcription factors such as Runx2 and osterix, which induce the expression of osteoblast marker genes such as alkaline phosphatase, type I collagen, and osteocalcin. However, the immune system plays also a key role in osteoblast differentiation. It has been proven that activated immune cells release soluble molecules, such as cytokines and signaling molecules, which strongly influence the osteogenic gene expression and differentiation of MSCs. [8] As such, monocytes have been shown to simulate hMSCs differentiation into osteoblasts by producing pro-osteogenic factors such as oncostatin M and by activating STAT3 signaling in osteoblasts through direct cell contact. [9]

Graphene-based nanomaterials can be design based on chemical-physical characteristics and functionalization, with the ability to induce different molecular impacts on the immune system. [10] In a previous study, it was demonstrated that a particular type of graphene oxide (GO) with small lateral dimension could induce a specific activation stimulus on monocytes. [10]

Based on these findings, we combined the distinctive activation proprieties of GO on monocytes and the well-recognized osteoinductive capacity of calcium phosphates (CaP) in a novel unique biocompatible nanomaterial called maGO-CaP (Monocytes Activator Graphene Oxide conjugated with Calcium Phosphates). In the present study, we analyzed the effect of maGO-CaP on osteogenic differentiation of MSCs *in vitro* and *in vivo* and assessed the underlying mechanisms. We

hypothesized that maGO-CaP promotes the MSC differentiation into osteoblasts through monocyte activation. Firstly, we evaluated the impact of maGO-CaP on monocytes and hMSC, analyzing cell viability and activation by flow cytometry. The ability to induce osteogenic differentiation of maGO-CaP was assessed studying osteoblastogenesis through the expression of osteogenic markers and the mineralization capacity *in vitro* and by assessing bone mass and bone formation *in vivo*. Furthermore, we analyzed Wnt and BMP signaling as potential underlying mechanisms. The ability of maGO-CaP to boost bone formation was confirmed by microcomputed tomography (μCT), histology and gene expression.

4.2 Materials and methods

4.2.1 Nanomaterials: synthesis and characterization

GO was purchased from NanoInnova (Spain) (batch no. NIT.GO.R.10.1) as a powder, produced by a modified Hummers' method. CaP and maGO-CaP were synthesized mixing two reverse microemulsions A and B. Emulsion A was prepared by mixing 200 µL of 100 mM CaCl2, in 2.65 ml of 30% Igepal CO-520 in cyclohexane. Emulsion B was prepared by mixing 200 µL of 60 mM Na2HPO4 in 2.65 ml of 30% Igepal CO-520 with 50 µl of DMF. To prepare maGO-CaP, we added 1 mg of GO to the phosphate solution before the addition of cyclohexane. To form a clear microemulsion, both emulsion A and B were mixed for 30 minutes. Therefore, microemulsion B was added dropwise to microemulsion A, mixing vigorously, until the formation of microemulsion C. Then, 50 µl of 1% Pluronic® F-127 in water solution was added slowly to the microemulsion C by mixing for 30 minutes. Subsequently, 16 ml of ethanol were added to destroy the emulsion and the CaP or maGO-CaP were separated by centrifugation at 5000 rpm for 10 minutes. After washing three times with ethanol and three times with water, CaP and maGO-CaP were kept in Milli-Q water for 20 days for maturation.
TEM images were obtained using a Hitachi H7500 microscope (Tokyo, Japan) with an accelerating voltage of 80 kV, equipped with an AMT Hamamatsu camera (Tokyo, Japan).

4.2.2 Cell culture

Buffy coats of healthy blood donors (25–50 years old) were collected from the University Hospital Carl Gustav Carus, Dresden. PBMCs were purified from whole blood using biocoll gradient centrifugation (1.077 g/ml, Biochrom). After PBMCs purification, monocytes were isolated using Dynabead Untouched™ Human Monocytes Kit (Invitrogen).
Bone marrow aspirates were obtained from healthy donors after completion of written informed consent, following Institutional Review Board approval (Uniklinikum, Dresden, Germany). Bone

marrow aspirates were diluted 1:5 in PBS and primary hMSCs were separated by biocoll solution (1.077 g/ml, Biochrom)

All the cells were cultured in Dulbecco's modified Eagle medium (DMEM)-low glucose supplemented with 1% of penicillin/streptomycin solution and 10% fetal calf serum, at 37°C under a humidified 5% CO_2 atmosphere.

hMSCs were co-cultured with monocytes at a ratio 1:10 in osteogenic medium: DMEM supplemented with 10 nM dexamethasone, 100 μM ascorbic acid 2-phosphate, and 10 mM β-glycerophosphate.

4.2.3 Apoptosis and viability assay

The apoptosis assay was performed using Annexin V/PI labeling (Invitrogen, Carlsbad, CA). Monocytes and hMSCs were incubated separately for 24 hours with increasing doses (5, 25, 50μg/ml) of GO, CaP, and maGO-CaP or left untreated. The cells were stained with Annexin V/PI staining, incubated for 20 minutes in the dark and suspended in Annexin V 1× buffer. As positive control, the cells were treated with ethanol at 70% before staining. AnnexinV, is a protein that binds phosphatidylserines (PS), which is "flipped" to the outer leaflet of the cell membrane during the early stages of apoptosis. The second component of the staining is PI, a dye molecule able to bind DNA, but it can only enter cells when their membranes are altered, which is a typical characteristic of necrosis. The late apoptosis presents PS at the extracellular side of the membrane but there is also loss of membrane integrity. At this stage, the cells are positive for both, Annexin V and PI. The cell fluorescence was measured by flow cytometry (LSR II BD Bioscience) and 50000 to 100000 events were collected.

The CellTiterBlue assay (Promega, Mannheim, Germany) was used to evaluate cell viability. This assay is based on the ability of viable cells to reduce resazurin into resorufin, which is highly fluorescent and can be detected by a spectrometer. Cells were seeded in 96-well plates in the presence or absence of increasing doses of GO, CaP, or maGO-CaP (5, 25, 50 μg/ml). After 24 hours the fluorescence intensity was measured using a microplate reader (FluoStar Omega (λex: 560 nm, λex: 590 nm; BMG).

4.2.4 Activation assay

Monocytes were cultured in 12 well-plates at the concentration of 1 x 10^6 cell/well. Monocytes were incubated with or without GO and maGO-CaP (5-25-50 μg/ml) or bacterial endotoxin lipopolysaccharides (LPS; 2 μg/ml), purchased from Sigma-Aldrich and used as the positive control. After 24 hours treatment, supernatants were collected to evaluate tumor necrosis factor-alpha (TNF-α) and interleukin 6 (IL-6) secretion using ELISA kit (Boster Biological Technology), while cells were stained to identify activation markers expression (CD69, CD25, CD80, and CD86, eBioscience). CD69, a member of the C-type lectin superfamily (Leu-23), is one of the earliest inducible cell surface glycoproteins expressed by immune cells during activation. CD25 is the alpha chain of the IL-2 receptor, a late activation antigen expressed by lymphomonocytes. The cluster of differentiation 80 (CD80) is a protein found on activated antigen-presenting cells such as B cells and monocytes that play an important role in T cell activation and survival. Staining with fluorochrome-conjugated monoclonal antibodies was performed in the dark for 20 minutes at 4°C. After washing, cells were analyzed by LSR II (BD Bioscience).

4.2.5 ALP and alizarin red S

hMSCs alone or co-cultured with monocytes were seeded in 24-well plates and treated with GO, CaP, and maGO-CaP (50 μg/ml) or left untreated. At day seven, cell lysates were incubated with an ALP substrate buffer (100 mM diethanolamine, 150 mM NaCl, 2 mM MgCl2, and 2.5 mg/ml p-nitrophenylphosphate). We used BCA method to determine protein concentration. Color change was measured using a spectrometer (Fluostar, BMG) at 405 nm and normalized to the total protein concentration.

To verify the bone matrix formation, we used alizarin red staining. The co-cultures were seeded in 48 well plates and, after 14 days of treatment, the cells were fixed with 70% ethanol and stained with 40 mM alizarin red S. After washing with distilled water, the plates were dried. The residual bound and stained calcium was then eluted using 100 mM cetylpyridinium chloride and quantified with a spectrometer at 540 nm.

4.2.6 Real-time PCR and osteogenesis array

After 14 days of treatment, RNA was isolated from co-culture using Trifast reagent (Invitrogen, Carlsbad, CA) and quantified using a Nanodrop spectrophotometer (Peqlab, Germany). Five-hundred nanograms of RNA were reverse transcribed using Superscript II (Life Technologies, Carlsbad, CA) and the expression of Runx2, Col1a, OCN, BMP6, Axin2, CD44 and LEF1 genes was analyzed using one step plus real-time PCR system from One Step Plus (Applied Biosystems, Foster City, CA). The results were calculated with 2-ΔΔCT method and were analyzed using β-actin as housekeeping gene. [11]

For the osteogenesis array, cDNA synthesis was obtained using Superscript IV Reverse Transcriptase kit (Life Technologies). RT2 Profiler PCR Array (PAHS-026Z, Qiagen Germany) was used to identify the expression of 84 osteogenesis-related genes. Amplifications on plates were performed by real-time PCR instrument (Applied Biosystems).

4.2.7 OSM and TLR2/4 evaluation in hMSCs differentiation

Supernatants were harvested from co-cultures of hMSCs-monocytes after seven days of treatment to measure secreted Oncostatin M (OSM) levels by Human OSM/Oncostatin M PicoKine™ ELISA Kit (Bosterbio).

To evaluate the role of OSM in the hMSCs differentiation process mediated by maGO-CaP, OSM neutralizing antibody (R&D System) was added or not added to the co-cultures at the concentration of 100 ng/ml in the osteogenic medium. Alizarin red assay was performed to analyze mineral deposition.

The co-cultures were pre-treated with anti-toll like receptor (TLR) 2 and anti-TLR4 antibodies for 30 minutes before incubation with 50 μg/ml maGO-CaP. Alizarin red staining was used to evaluate the bone matrix formation in the presence or the absence of anti-TLR2 and anti-TLR4 after 14 days of treatment with maGO-CaP. At day seven, the supernatant samples were collected to analyze the OSM secretion by Human OSM/Oncostatin M PicoKine™ ELISA Kit (Bosterbio).

4.2.8 Mice

Thirty C57BL/6 mice, 12-weeks-old male, were received from Janvier (France). Study procedures were approved by the Institutional Animal Care Committee and the Landesdirektion Sachsen. The mice were divided into two groups: control and treated with maGO-CaP. A hole was drilled into the tibia using a 27G × ¾ 0.4 × 19 mm needle and 20 µl of 50 µg/ml maGO-Cap or PBS as a negative were injected intratibially. After one week or four weeks, mice were sacrificed to assess bio-immune compatibility and local bone turnover.

4.2.9 Flow cytometric analysis of immune cells

After seven days and one month of injection, the spleen, the lymph nodes, the thymus, and the bone marrow were harvested. To create cell suspension, the tissues were mechanically dissociated by gentle trituration and filtered through a cell strainer. Major immune cell populations were analyzed using flow cytometry according to the expression of specific cell surface markers, detected with fluorochrome-conjugated monoclonal antibodies. Cells were washed twice with 0.5% bovine serum albumin in PBS pH 7.2 and were incubated for 20 minutes in the dark with fluorescently labeled antibodies. Cell typing was performed using CD45 for leukocytes, CD3 for T cells, CD4 for T helper, CD8 for T killer, CD11b for myeloid cells, CD11c for dendritic cells and Gr1 for granulocytes.

4.2.10 µCT measurement

The bone formation of tibias was evaluated *ex vivo* by microcomputed tomography using a vivaCT40 (Scanco, Switzerland). The bones were scanned at a resolution of 10.5 µm and 200 ms integration time. The contours of trabecular bone were taken by hand and pre-defined scripts from Scanco were used for the analysis. According to the international guidelines [12] we evaluated the trabecular bone volume/total volume (BV/TV), trabecular number (Tb.N) and the trabecular thickness (Tb.Th).

4.2.11 Bone histology

To determine bone formation parameters, five and two days before sacrifice, mice received a calcein injection (20 mg/kg) intraperitoneally to later identify newly formed bone. After sacrifice, the tibias were fixed in 4% PBS-buffered paraformaldehyde and dehydrated in an ascending ethanol series. Then, bones were embedded in methacrylate and cut into 7 μm sections. The sections were analyzed using fluorescence microscopy to assess the fluorescent calcein labels. Dynamic bone histomorphometry was performed to determine the mineralized surface/bone surface (MS/BS), the mineral apposition rate (MAR), and the bone formation rate/bone surface (BFR/BS).
Moreover, the femur of each mouse was fixed in 4% PBS-buffered paraformaldehyde, decalcified for one week using Osteosoft (Merck, Germany), dehydrated using ascending series of ethanol and embedded with paraffin. For these analyses, the bones were cut into 4 μm sections and stained for tartrate-resistant acid phosphatase (TRAP) to identify osteoclasts and osteoblasts. Histomorphometric analysis was carried out using Osteomeasure software (OsteoMetrics, USA), according to international standards. [13]

4.2.12 Statistical analysis

All experiments were performed at least in triplicate. Statistics of experiments were evaluated using one-way ANOVA or Student's *t*-test. P-values<0.05 were considered statistically significant. Flow cytometry data were analyzed with FlowJo software. The comparative threshold cycle method was used to calculate immune gene array data. Data were analyzed using RT2 profiler PCR array data analysis software from Qiagen.

4.3 Results and discussion

4.3.1 Synthesis of maGO-CaP and cell viability

Firstly, we prepared CaP as described in the literature. [4] Subsequently, we employed the reverse emulsion method using Pluronic F127 as a capping agent to obtain CaP amorphous nanoparticles. maGO-CaP were then synthesized by adding the GO flakes in the synthetic batch. The **Figure 1** shows the TEM microscopy images of CaP and maGO-CaP.

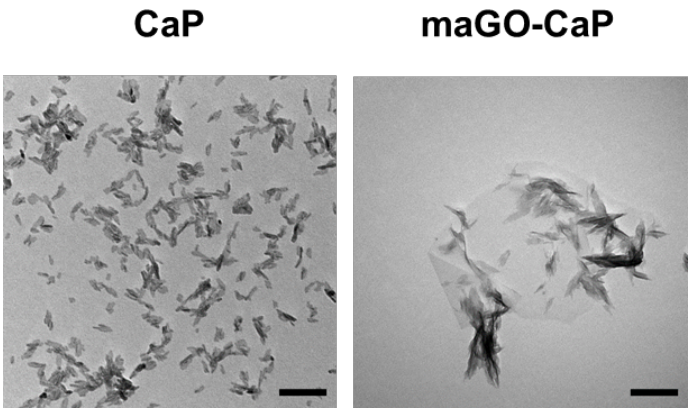

Figure 1. Morphology of maGO-CaP. TEM images of mature CaP and ma-GOCaP (scale bar: 200nm)

Several studies were performed to evaluate the biocompatibility of graphene, founding contradictory results. [14] Some investigation demonstrated the high biocompatibility of graphene, with no compromise in cell viability. [15, 16] On the other hand, some manuscripts reported cytotoxicity effects after graphene treatment, associated with increase of apoptosis and necrosis. [17, 18] These contradictions are the results of different graphene materials used for the analysis. Indeed, several factors, including lateral size dimension, shape, thickness, stiffness, surface functionalization,

concentration and time of exposure to cells, influence the different impacts on cell. [19] Therefore, we firstly evaluated the impact of maGO-CaP on cell viability.

Monocytes, isolated from PBMCs, were exposed to increasing doses of GO, maGO-CaP or CaP (5, 25, 50 μg/ml). To assess early apoptosis, late apoptosis and necrosis, we used AnnexinV/propidium iodide (PI) staining (**Figure 2A**). No significant difference was found in the percentage of apoptotic and necrotic cells, also after treatment with the highest concentrations used (50 μg/ml) (**Figure 2A**). We confirmed the data using CellTiter Blue assay (**Figure 2B**).

The impact of nanomaterials on hMSCs was studied as above reported for monocytes. Using Annexin V/PI staining we demonstrated that maGO-CaP did not affect hMSCs viability (**Figure 2C**). Similarly, we did not find any significant difference in fluorescence intensity between untreated and treated cells using CelTiter Blue assay (**Figure 2D**). These results are in agreement with other authors who reported a good biocompatibility of graphene-based materials on progenitor cells, including MSCs. [20, 21] Zancanela et al. i.e. investigated the effects of GO on osteoblast viability at one and five days selecting GO concentrations of 25 and 50 μg/mL. They found higher cell viability compared to the controls, highlighting also increased cell growth after one day of incubation. [22]

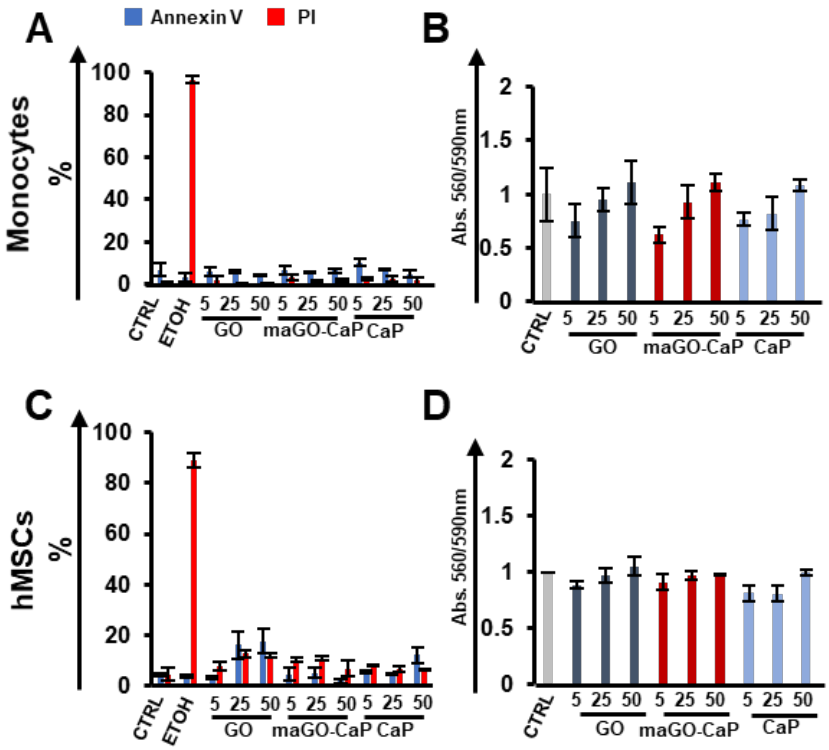

Figure 2. Cell viability. B) and C) Monocytes, isolated from PBMCs, were treated with increasing doses of GO, maGO-CaP and CaP (5, 25, 50 µg/ml) for 24 hours or left untreated. B) Viability was assessed by flow cytometry using Annexin V and PI staining. C) CellTiter-Blue assay was performed to confirm cell viability impact after treatment with each material. D) and E) hMSCs, isolated from bone marrow of healthy donors, were cultured in presence of increasing doses of GO, maGO-CaP and CaP (5, 25, 50 µg/ml) for 24 hours or left untreated. The same assays used for monocytes were performed: D) Annexin V/PI staining. E) CellTiter Blue assay.

4.3.2 Monocytes Activation

As activated monocytes were shown to stimulate the function of osteoblasts, [8, 23, 24] we investigated the ability of maGO-CaP to activate monocytes as previously shown for GO. [10] Therefore, monocytes were exposed for 24 hours to GO or maGO-CaP (5, 25, 50 μg/mL) and the expression of the main immune activation markers was evaluated by flow cytometry (**Figure 3A**). In particular, we analyzed the expression of CD69, CD25 and CD80. After GO and maGO-CaP treatment, these markers were found highly expressed compared to control samples, confirming maGO-CaP activation action on monocytes (**Figure 3A**). We found a statistically significant induction of CD25 and CD80 (P-value < 0.01), demonstrating that maGO-CaP maintained the immune-characteristics of GO (**Figure 3A**). To confirm the monocytes activation status, we evaluated the levels of TNFα and IL-6 in the cell supernatants (**Figure 3B**). IL-6 and TNFα are cytokines secreted by monocytes/macrophages and related to the innate immune system response. According to our results, Zhi et al. showed that the incubation with GO induced a specific stimulus on the innate immune system with the release of primary proinflammatory cytokines such as IL-6, TNFα and IL1β. [25]

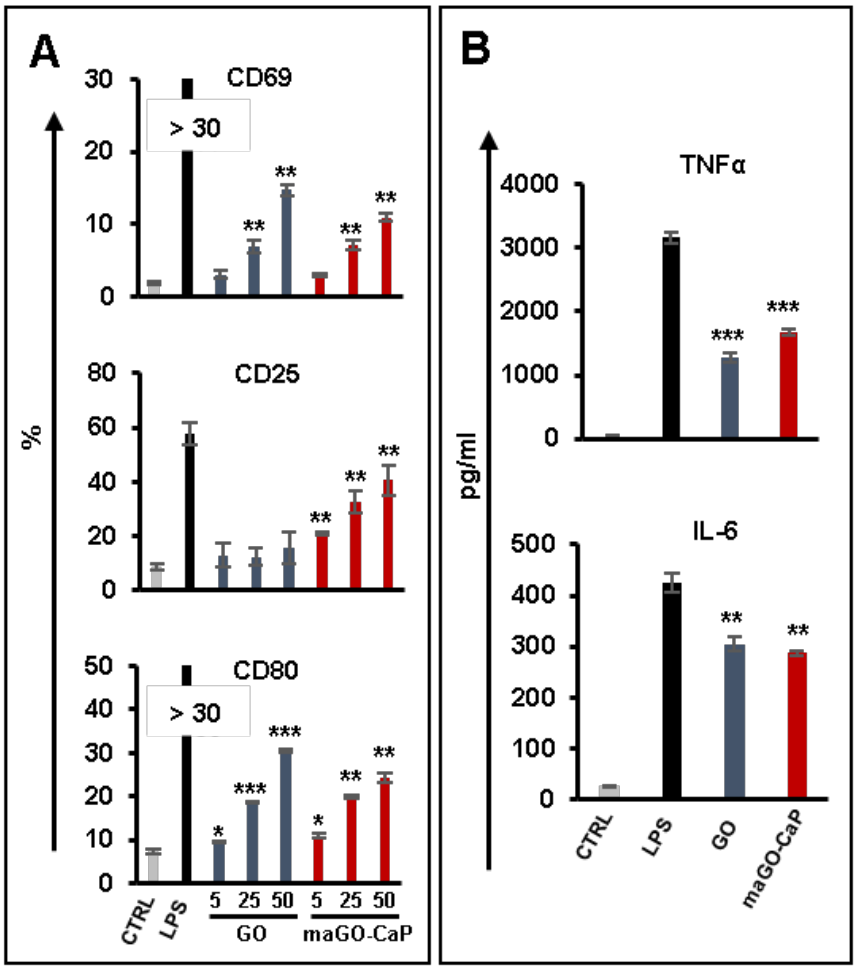

Figure 3. Monocyte activation. Monocytes were incubated for 24 hours with increasing doses of GO and maGO-CaP (5, 25, 50 µg/ml) or left untreated. A) The activation of monocytes was analyzed by flow cytometry using three main activation markers: CD69, CD25 and CD80. B) To evaluated TNFα and IL-6 secretion, cells were treated with 50 µg/ml of GO and maGO-CaP or left untreated and the supernatant was analyzed by ELISA. LPS (2 µg/ml) was used as positive control. Data were analyzed using Student's t-test, *=p value<0.05, **=p value<0.01, ***=p value<0.001.

4.3.3 Osteoblast differentiation in the presence of monocytes

The osteogenic process is strictly correlated to monocytes, which interact directly with MSCs through cell contacts or release pro-osteogenic mediators, such as oncostatin M (OSM). [9, 26, 27]

We hypothesized that maGO-CaP could stimulate monocytes to express these factors, inducing hMSCs differentiation. Therefore, we performed a co-culture of human monocytes and hMSC at 10:1 ratio, as found in literature, and we treated it with GO, Cap and maGO-CaP. Considering 50 µg/ml of maGO-CaP as the best concentration able to induce osteoblast differentiation, we evaluated the alkaline phosphatase (ALP) activity (**Figure 4**). ALP is an important enzyme involved in hard tissue formation, highly expressed in mineralized tissue cells. ALP is implicated in the dephosphorylation process of several types of molecules and the increase of its activity is an index of the MSCs differentiation into osteoblasts. [28, 29, 30, 31, 32] After seven days of treatment with maGO-CaP, ALP activity was significantly increased compared to negative controls and samples treated with only CaP and GO (p value<0.01) (**Figure 4**).

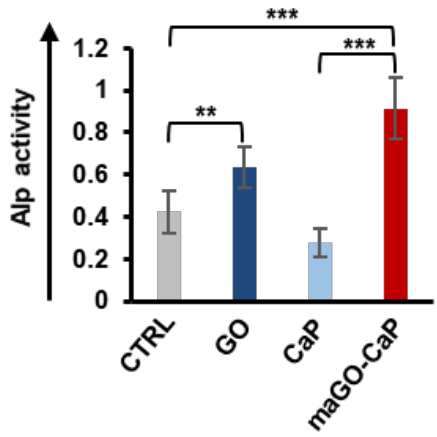

Figure 4. ALP activity. Co-cultures of hMSCs-monocytes, at 1:10 ratio, were incubated with 50 µg/ml of GO, CaP and maGO-CaP or left untreated. ALP activity was quantified at day seven.

The maGO-CaP propriety inducing osteogenesis was confirmed by analysis of the bone matrix formation using Alizarin Red S staining (**Figure 5**). The data showed a significant increase of absorbance intensity when hMSCs-monocytes were grown in the presence of 50 µg/ml of maGO-CaP respect to the untreated control condition.

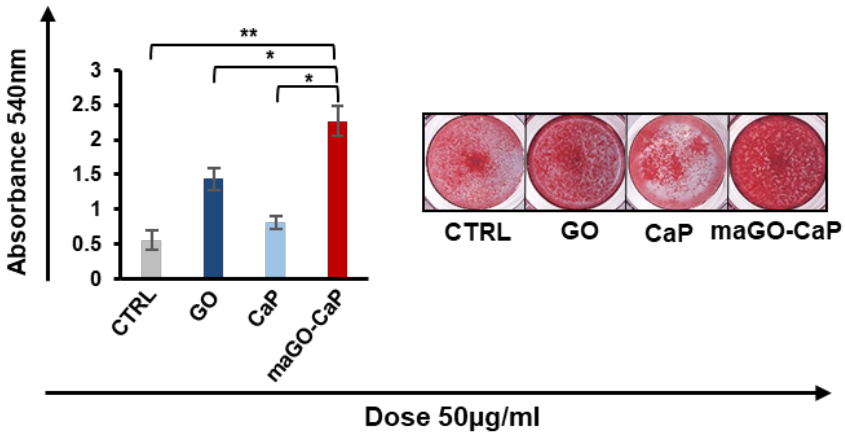

Figure 5. Alizarin Red assay. After 14 days of treatment with 50 µg/ml of GO, CaP and maGO-CaP, Alizarin Red Staining was performed to visualize the bone matrix formation.

In hMSC only cultures, maGO-CaP effects on ALP activity and mineralization were reduced compared to co-culture (**Figure 6A and 6B**), suggesting that the additive effect observed in the co-culture is likely to be mediated *via* monocytes activation.

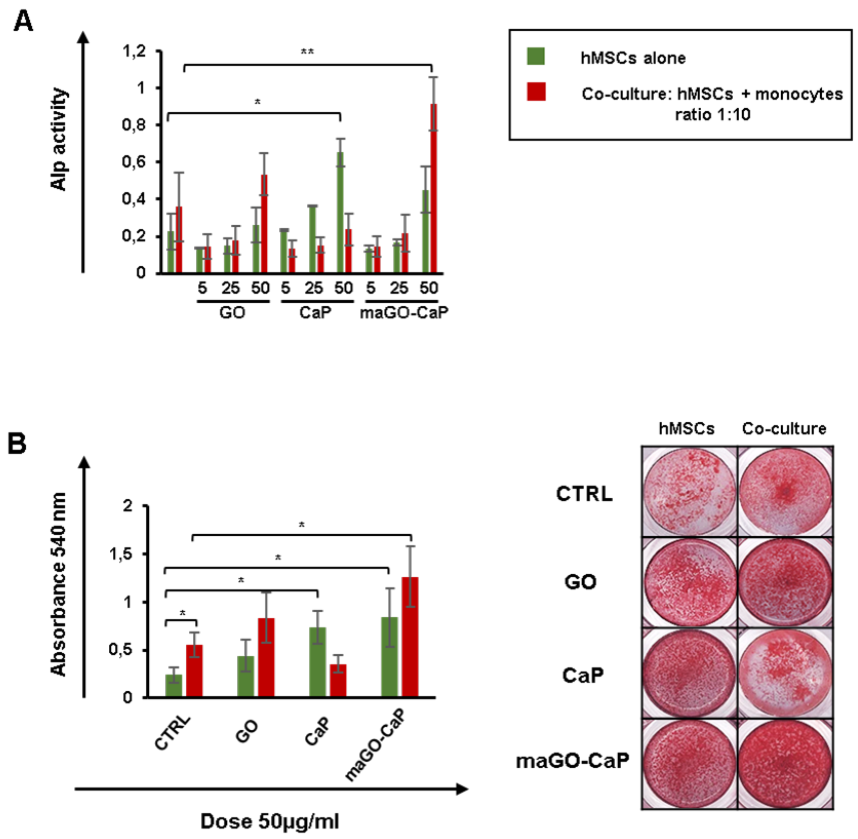

Figure 6. Osteogenic differentiation of hMSCs in the presence or absence of monocytes. hMSCs-monocytes co-cultures and only hMSCs without monocytes were grown in presence of GO, CaP and maGO-CaP or left untreated. A) After seven days of treatment, ALP activity was analyzed. B) To evaluate the bone matrix formation, Alizarin Red assay was performed at day 14. Data were analyzed using ANOVA test and Student's t-test, *=p value<0.05, **= p value<0.01, ***=p value<0.001.

These outcomes could be a demonstration that GO enhances in a synergistic way the osteoinductive capacity of CaP. The augment of osteogenic effects on hMSCs is a specific characteristic of the compound formed by GO and CaP. Tatavarty et al. demonstrated that GO-CaP exhibited osteogenic capability that was superior to individual or combined effects of GO and CaP. [4] As a contribution of this study, we underlined the correlation between monocyte responses to maGO-CaP interactions and

osteoblast differentiation. Therefore, we can assume that maGO-CaP has a direct action on hMSCs, boosting the osteogenic proprieties of CaP, and an indirect action on osteoblastogenesis, stimulating monocytes activation thanks to the presence of GO.

To further validate these data, we investigated the influence of maGO-CaP on osteogenic gene expression of hMSCs. We analyzed four key osteogenic genes in the co-culture: runt-related transcription factor (Runx2), collagen type 1 (Col1a), osteocalcin (OCN) and bone morphogenic proteins 6 (BMP6) (**Figure 7**).

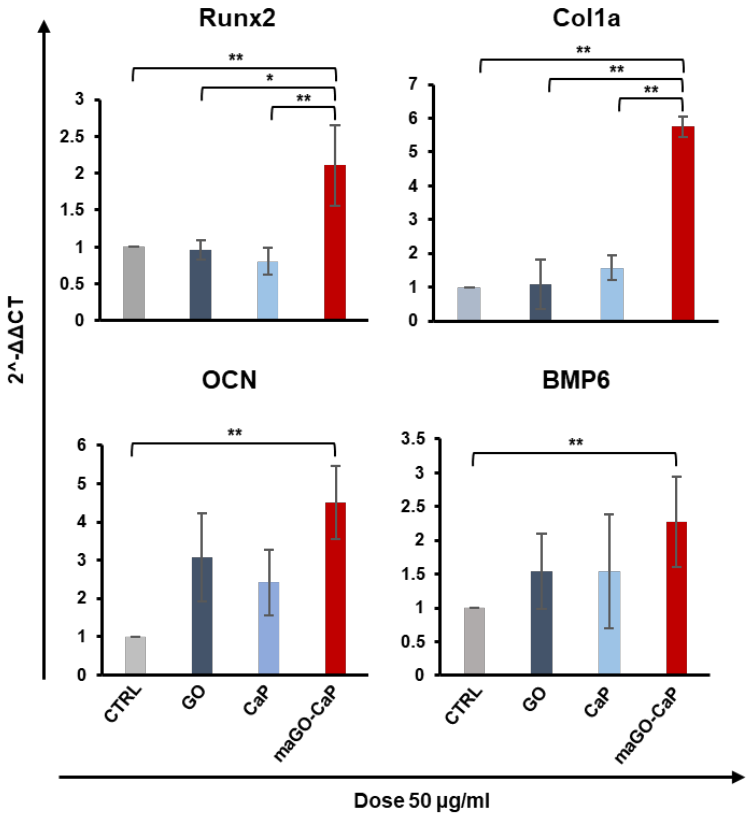

Figure 7. Gene expression. Runx2, Col1a, OCN and BMP6, the main osteogenic genes, were analyzed by Real-Time PCR. Data were analyzed using ANOVA test and Student's t-test, *=p value<0.05, **= p value<0.01, ***=p value<0.001.

Runx2 encodes for transcription factors that leads the expression of osteoblast marker genes, including Col1a and OCN. Collagen genes, including Col1a, are associated with extracellular matrix (ECM), which is a central component of cellular microenvironments in bone. Col1a influences the expression of osteoblastic phenotypes by extracellular signals. OCN, also known as bone gamma-carboxyglutamic acid-containing protein (BGLAP), is a non-collagenous protein found in bone and dentin. OCN is involved in bone mineralization and calcium ion homeostasis. BMPs are family of signaling proteins able to induce the growth of bone, stimulating the expression of osteogenic markers in MSCs.

Figure 7 shows the relevant up-regulation of Runx2, Col1a, OCN and BMP6 genes after two weeks' exposure of 50μg/ml GO-CaP compared to untreated samples (p value<0.001). Interestingly, we found an over-expression of Runx2 and also Col1a mediated by maGO-CaP treatment compared to CaP samples (p value<0.01).

Our results are supported by other studies showing the potential of graphene to induce gene and protein expression of Runx2, Col1 and OCN without any addition of chemical inducers. [33, 34]

These results show the pro-osteogenic proprieties of maGO-CaP, highlighting its role in the crosstalk between monocytes and bone cells.

4.3.4 maGO-CaP osteogenesis mechanisms

To deeply understand the action of maGO-CaP on osteogenesis processes, we assessed the expression of specific genes involved in the Wnt pathway. [35] The Wnt pathway is a signal transduction pathway, consisting of several receptors, inhibitors, activators, modulators, phosphatases and kinases, involved in numerous aspects of growth and development in many organs and tissues, such as cell behavior, cell adhesion and cell polarity. [36] The Wnt signaling pathway is further separated in: I) the canonical

Wnt/β-catenin pathway, depending on the function of β-catenin and II) the non-canonical Wnt/Ca^{2+} pathway, independent from β-catenin. The components of Wnt/β-catenin signaling pathway are involved in MSCs regeneration, osteoblastogenesis and pre-osteoblast replication correlated to apoptosis inhibition. [37] Therefore, we evaluated the expression of three main genes associated to Wnt/β-catenin pathway in the co-culture: axin inhibition protein 2 (Axin2), CD44 and lymphoid enhancer-binding factor 1 (LEF1) (**Figure 8**). Axin2 is involved in the regulation of beta-catenin stability. [38] CD44 antigen is a receptor for hyaluronic acid, activated by beta-catenin and Wnt signaling. [39] LEF1 is a transcription factor that promotes the transcription of target genes related to Wnt signaling pathway. [40]

We found a statistically significant over-expression of Axin 2 (p value<0.05), CD44 (p value<0.05) and LEF1 (p value<0.01) after treatment with 50µg/ml maGO-CaP, demonstrating that osteoanabolic action of graphene may be at least partly mediated by the Wnt pathway (**Figure 8**).

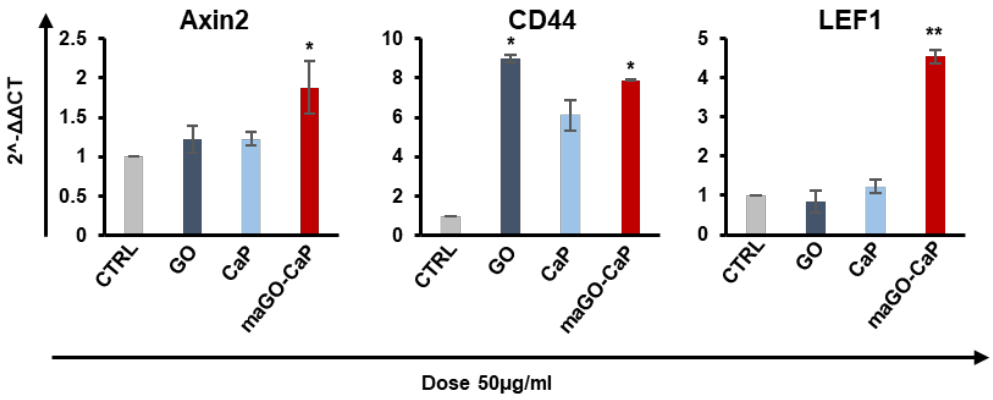

Figure 8. Wnt pathway. The main genes involved in the Wnt pathway were evaluated by Real-Time PCR. Data were analyzed using Student's t test, *=p value<0.05, **= p value<0.01.

To have a wide overview on the effects of maGO-CaP on key pathways involved in the osteo-differentiation process, we performed a deep genomic analysis on the expression of highly selected genes. PCR arrays on co-culture samples were performed to assess the expression of 84 key genes related to cell growth, proliferation and differentiation, bone formation and bone mineral metabolism. **Figure 9** shows the heat map details, with strong up-regulation of specific genes in response to maGO-CaP treatment. The pro-osteogenic potential of maGO-CaP was manifested by the over-expression of bone morphogenetic proteins (BMPs), a group of growth factors associated with the development of bone mineralization, with a fold change higher than 2. In particular, we found a significant increase in the expression of the following BMPs genes: BMP2 (4.71 fold-change), BMP3 (4.31-fold change), BMP4 (2.12-fold change), BMP6 (2.26-fold change) and BMP7 (2.38-fold change) (**Figure 9**). Correlated to BMPs signaling, we found an up-regulation also of expression of Smad1 (Mothers Against DPP Homolog 1) (**Figure 9**). Moreover, maGO-CaP treatment induced an overexpression of collagen genes, including Col10a1 (4.36-fold change), Col14a1 (3.22-fold change), Col1a2 (2.85-fold change) (**Figure 9**). The results obtained with the osteo-array were in line with gene expression analyzed by real-time PCR (**Figure 9**).

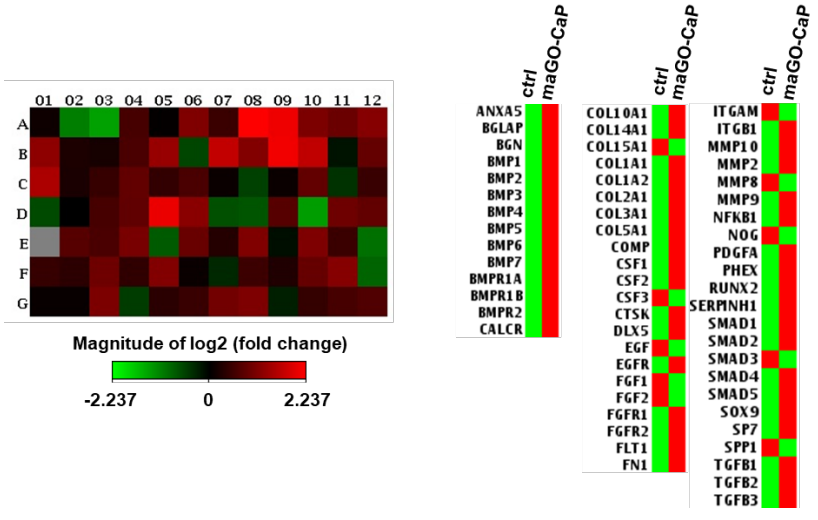

Figure 9. Osteogenic array. The experiments were carried out at least in triplicate and the data are reported as mean. Genes are showed for fold-change variations compared to the controls. The differences in gene expression are displayed using standardized color value: red = high expression; green = low expression. Heat-map detail indicates the osteo-differentiation genes up-regulated by maGO-CaP.

4.3.5 Osteogenesis process mediated by maGO-CaP: the role of monocytes

To confirm the key role of monocytes in MSCs differentiation process, we analyzed the expression of Oncostatin M (OSM), a cytokine released by activated monocytes/macrophage considered one of the major mediators able to promote osteogenesis in hMSCs. [9, 27, 41] OSM induces the differentiation of MSCs into osteoblast lineage, showing anti-adipogenic effects. [42, 43] During early stages of fracture healing, OSM is expressed by monocytes/macrophages and supports osteoblast differentiation by encouraging the recruitment and proliferation of MSCs. [44] Therefore, the role of OSM is crucial in the crosstalk between monocytes and bone cells. [45]

To evaluate whether OSM signaling could be involved in the osteogenesis of hMSCs driven by maGO-CaP, an ELISA assay was performed on supernatants of hMSC-monocyte co-cultures. OSM levels were significantly higher (p-value < 0.0001) in cells treated with maGO-CaP compared to untreated cells (**Figure 10**).

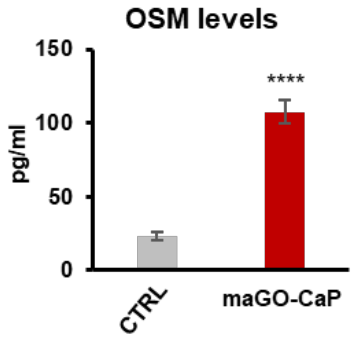

Figure 10. OSM levels. After seven days of treatment with 50 µg/ml of maGO-CaP, supernatants were collected and OSM levels were evaluated by ELISA (*=p value<0.05, **= p value<0.01, ***= p value<0.001, ****=p value<0.0001).

Consequently, to analyze the influence of these high levels of OSM on hMSCs differentiation, we used OSM neutralizing antibodies, adding them to co-culture at the concentration of 100ng/ml (**Figure 11**). By Alizarin Red Staining we analyzed the bone nodule formation, observing a decrease in the co-culture pre-treated with OSM neutralizing antibodies. These interesting results suggest the key role of OSM in the osteogenic process induced by maGO-CaP.

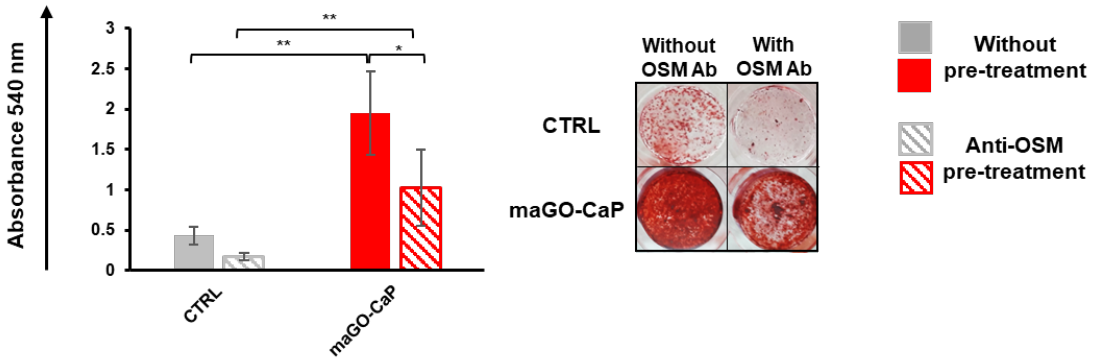

Figure 11. OSM and bone formation. hMSCs-monocytes co-cultures were grown in presence or absence of 50 µg/ml of maGO-CaP. Before treatment, OSM neutralizing antibodies (100 µg/ml). were added or not to co-cultures. To evaluate bone nodule formation, Alizarin Red Staining at 14 days was used (*=p value<0.05, **= p value<0.01).

The cell interaction mechanism of graphene with monocytes is still not clear. Graphene might elicit a Toll-like receptor (TLR)-mediated inflammatory response. TLRs are single membrane receptors involved in the innate immune system by activating immune cell responses. [46] Several studies observed the activation of macrophage cell lines mediated by GO through the interaction with TLRs, specifically TLR4 and TLR9. [47, 48, 49] Recently, a new chemically exfoliated few layers graphene was found able to cause necrotic pathways initiation in neoplastic monocytes by TLR2 and TLR4 receptors. [50] However, the TLRs interaction of graphene needs further experimental confirmations. To evaluate the key role of TLR2 and TLR4 in the activation of monocytes in response to maGO-CaP, we pre-treated the cells with TLR2 and TLR4 blocking antibodies before incubation with maGO-CaP (50µg/ml). In monocytes pre-treated with anti-TLR2 we found value of CD69, CD25 and CD80 expression similar to sample without pre-treatment. Interestingly, in samples pre-treated with anti-TRL4 a reduction of the expression of these activation markers was observed (**Figure 12**).

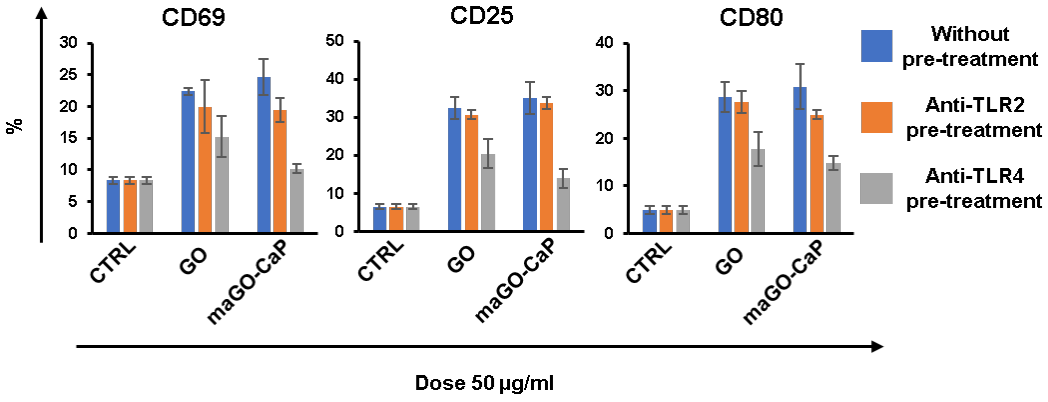

Figure 12. TLR and monocytes activation mediated by maGO-CaP. Monocytes were incubated with 50 µg/ml of GO and maGO-CaP. 30 minutes before incubation, blocking antibodies to TLR2

and TRL4 were added or not added to cultures. Flow cytometry was employed to evaluate the expression of CD69, CD25 and CD80.

Therefore, the levels of OSM were evaluated in the co-culture pre-treated with anti-TLR2 and anti-TLR4 antibodies (**Figure 13**). OSM release was still promoted in co-culture pre-treated with TLR2. On the other hand, in the sample pre-treated with anti-TLR4 we did not find any differences in OSM expression. These outcomes showed the role of TLR4, but not TLR2, in driving maGO-CaP to promote monocytes activation (**Figure 13**). In line with our results, several studies demonstrated that the activation of TLRs, through the interaction with exogenous or endogenous ligands, promotes the release of OSM by monocytes, boosting bone formation. [27, 51, 52]

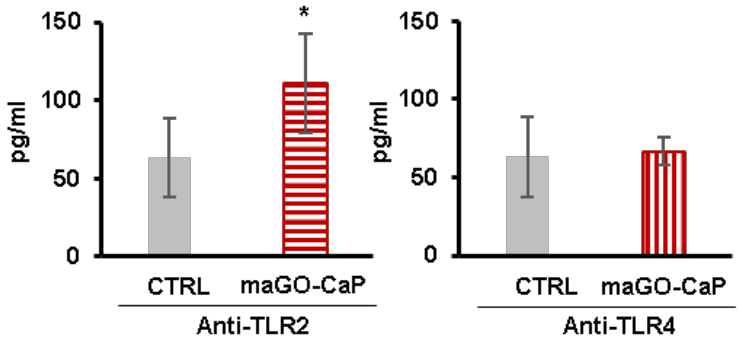

Figure 13. Anti-TLR2/4 and OSM levels. hMSC-monocyte co-cultures were pre-treated with anti-TLR2 and anti-TRL4 antibodies. After 30 minutes, cells were incubated with 50 µg/ml maGO-CaP. At day seven, OSM expression was analyzed in the cell culture supernatants by ELISA (*=p value<0.05).

To verify the correlation between TLRs activation and osteogenesis, we pre-treated the co-culture with anti-TLR2 and anti-TLR4 before incubation with maGO-CaP and we evaluated the bone nodule

formation by Alizarin Red Staining. As we expected, we found a high bone matrix formation in the co-culture pre-treated with anti-TLR2 was observed in comparison to control conditions (p value<0.01), values comparable to samples without pre-treatment (**Figure 14**). Interestingly, the bone nodule formation decreased blocking TLR4 before exposure of maGO-CaP compared to samples pre-treated with anti-TLR2 (**Figure 14**).

Based on these findings we can assume that the activation of monocytes by maGO-CaP is partly related to TLR4, which is correlated to OSM release and, consequently, to osteogenesis.

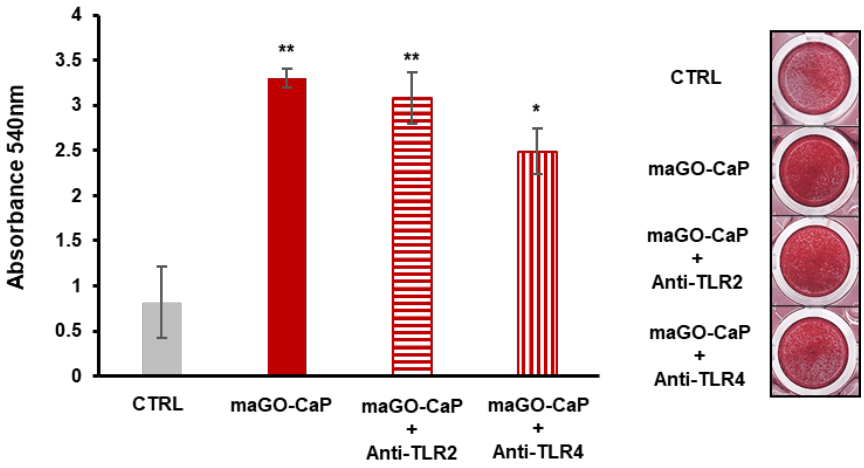

Figure 14. TLR role in bone regeneration. In the hMSCs-monocytes co-cultures, TLR2 and TLR4 were blocking or not blocking with corresponding antibodies with monocytes. Cells were then treated with maGO-CaP and bone nodule formation was analyzed after 14 days (p value<0.05, **= p value<0.01).

4.3.6 *In vivo* bone formation

12-week-old C57BL/6 male mice were treated with intratibial injection of 50 µg/ml of maGO-CaP or PBS as negative control to investigate whether maGO-CaP has also osteoblast-promoting effects *in vivo*. Firstly, we analyzed the *in vivo* biocompatibility of maGO-CaP (**Figure 15**). After seven days

and after one month of treatment, we did not find any differences in percentage of inflammatory cells present in spleen, lymph nodes, thymus and bone marrow between mice treated and control group (**Figure 15**).

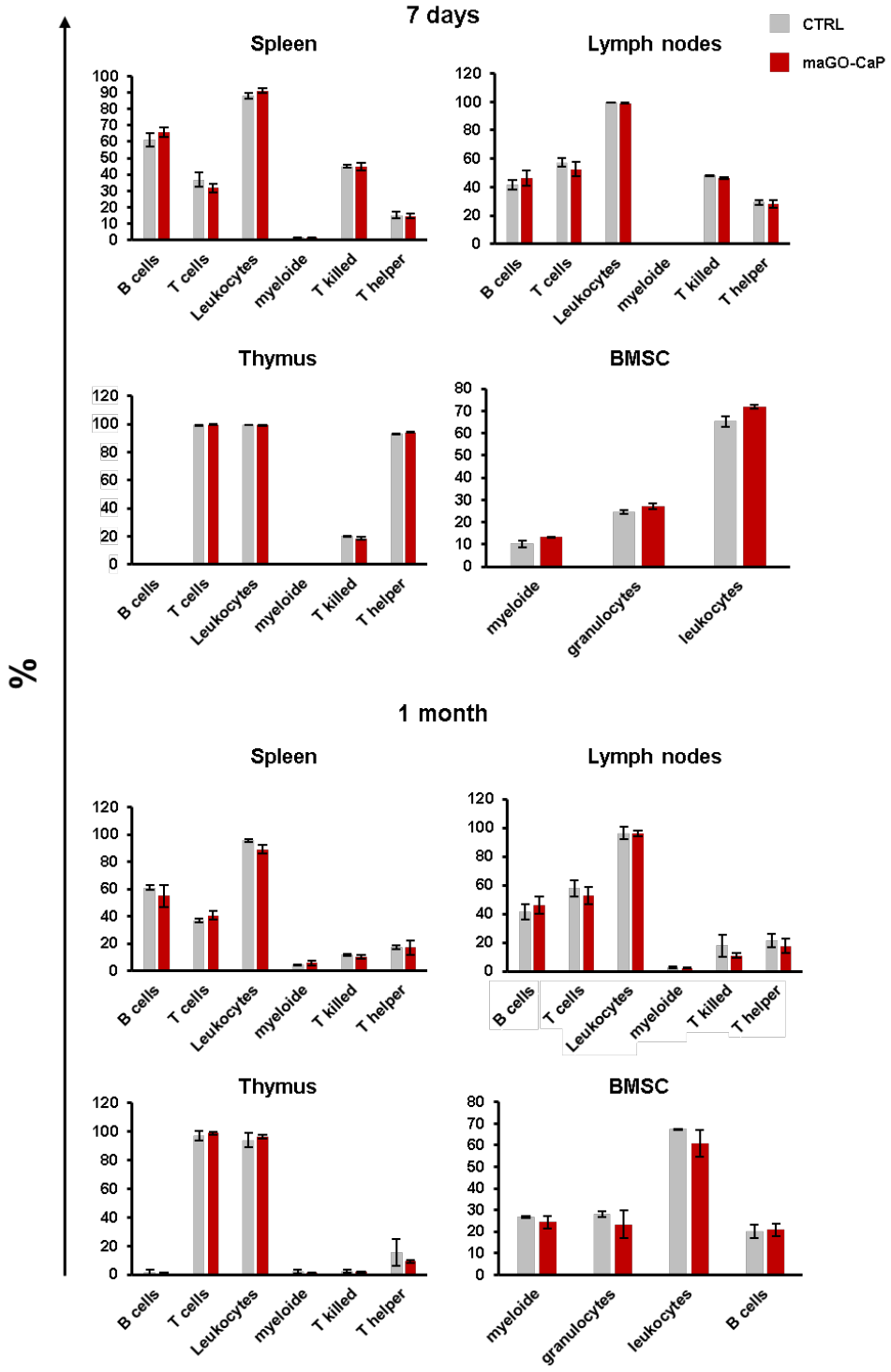

Figure 15. Systemic inflammation *in vivo*. Mice were sacrificed after one week and one month of treatment with maGO-CaP. Spleen, lymph nodes, thymus and bone marrow were harvested. The main immune cell populations, involved in inflammatory reactions, was analyzed by flow cytometry.

Table 1 shows blood analysis, revealing similar values of red blood cells, the hematocrit, platelets and all subpopulations of white blood cells between the control and maGO-CaP groups. In treatment, maGO-CaP was well tolerated *in vivo*, without evoked systemic inflammation and side-effects.

	PBS mean value	maGO-CaP mean value	P value	St Dev
Red Blood Cells $[10^{12/L}]$	9.43	9.164	0.448	0.188
Haematocrit [Ratio]	0.469	0.456	0.459	0.009
Platelet $[10^{9/L}]$	804.5	807	0.420	112.297
White Blood Cells $[10^{9/L}]$	4.99	4.584	0.446	0.287
Neutrophil $[10^{9/L}]$	0.575	0.568	0.939	0.004
Lymphocytes $[10^{9/L}]$	4.28	3.904	0.504	0.265
Monocytes $[10^{9/L}]$	0.13	0.112	0.638	0.012

Table1. Blood analysis.

To assess if maGO-CaP is able to induce bone formation and thus bone mass, three-dimensional μCT measurements of the tibias were performed *ex vivo*. **Figure 16** shows the differences in bone characteristics: a statistically substantial increase of trabecular number (Tb.N) (p value<0.05), trabecular thickness (Tb.Th) (p value<0.05) and significant trabecular bone volume fraction (BV/TV)

(p value<0.01) was found in the tibias of mice treated with maGO-CaP. Thanks to μCT images, it is possible to observe the enhancement after maGO-CaP treatment (**Figure 16**).

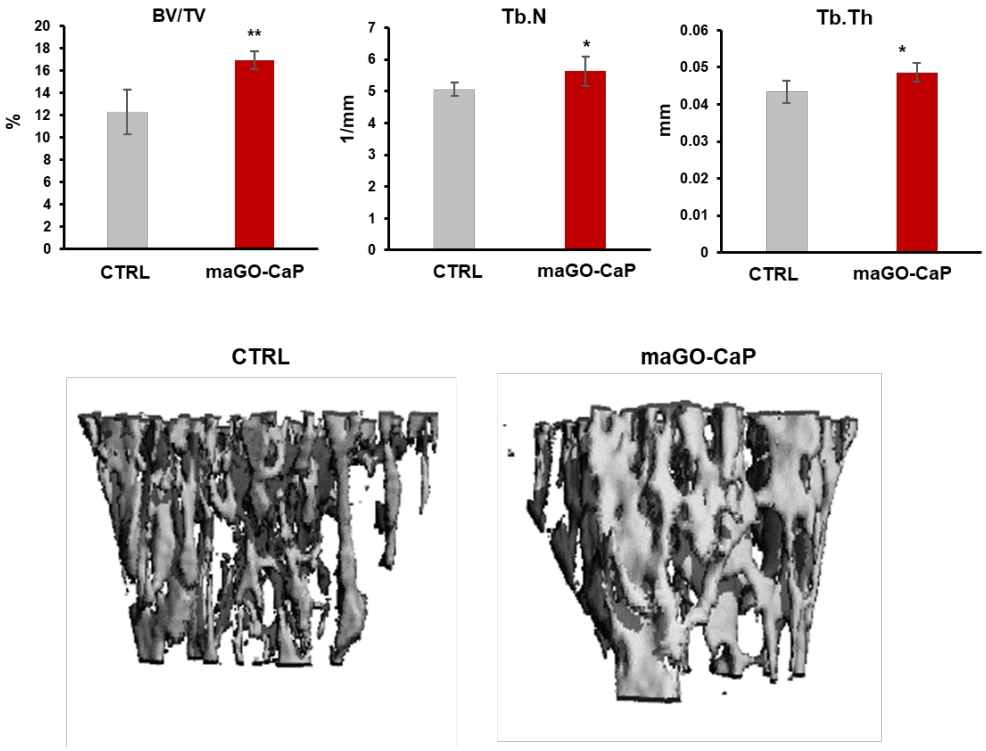

Figure 16. μCT analysis. Tibias of 15 mice (five per group) were analyzed by microcomputed tomography (μCT) after one-month treatment. The histograms show the following values: the ratio between trabecular bone volume and total volume (BV/TV), trabecular number (TB.N) and trabecular thickness (TB.Th). Below, the μCT images of untreated tibia (CTRL) and tibia treated with maGO-CaP. Data were analyzed using ANOVA test, *= p value<0.05, **= p value<0.01.

The pro-osteogenic properties of maGO-CaP were also investigated in sections of bone stained with tartrate-resistant acid phosphatase (TRAP) to analyze the number of osteoblasts and osteoclasts using the Osteomeasure. The osteoclasts are multinuclear cells responsible for bone resorption. maGO-CaP

treatment did not affect the number of osteoclasts for the bone perimeter. However, the number of osteoblasts increased in mice treated with maGO-CaP (**Figure 17**).

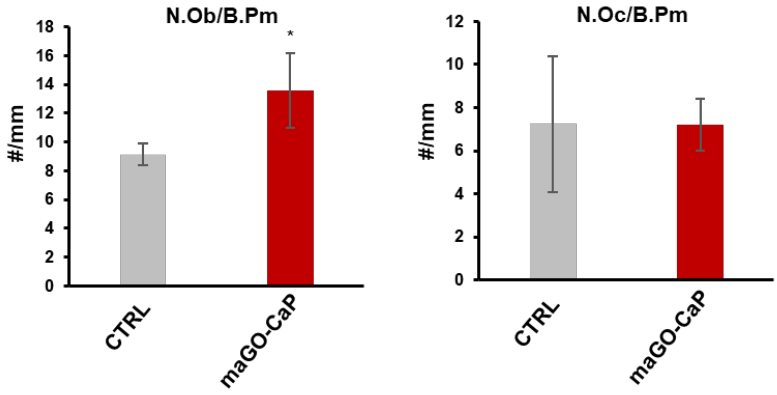

Figure 17. TRAP staining. TRAP staining was performed in histology sections of bone in order to measure the number of osteoblasts per perimeter bone and the number of osteoclasts per perimeter bone. Data were analyzed using Student's *t*-test (*= p value<0.05).

Regarding the osteoblasts per bone surface, using dynamic bone histomorphometry, we found a significant rise of mineralized surface (p value<0.05). Moreover, the bone formation rate (p value<0.05) was enhanced in maGO-CaP-treated mice compared to the controls (**Figure 18**).

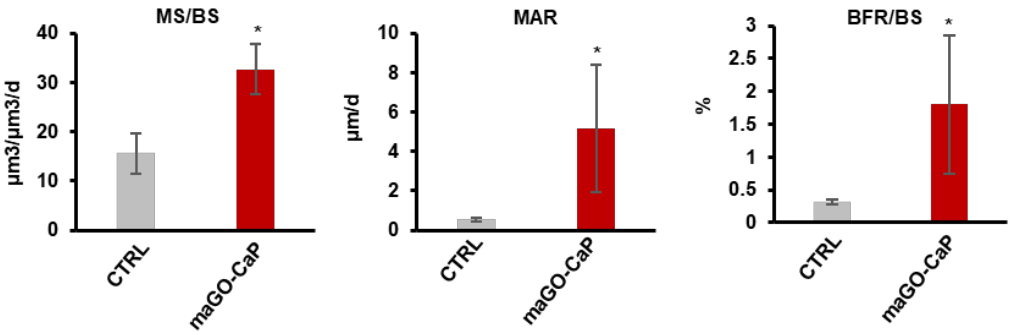

Figure 18. Dynamic bone histomorphometry. 5- and 2-days mice were injected with 20 mg/kg calcein before sacrifice. Bone sections were prepared and analyzed using fluorescence microscopy. The mineralized surface/bone surface (MS/BS), the mineral apposition rate (MAR), and the bone formation rate/bone surface (BFR/BS) was determined (*= p value<0.05).

Moreover, to investigate the effects on gene expression after injection with maGO-CaP, we performed osteogenesis arrays on bone marrow cells (**Figure 19**). These analyses allow us to evaluate the expression of 84 bone formation-related genes. We found results comparable to *ex vivo* experiments, with up-regulation collagens genes, including Col1a1 (2.85-fold) and Col1a2 (4.16-fold), biglycan (Bgn 2.66-fold change) and osteocalcin (Bglap 2.20-fold change) (**Figure 19**).

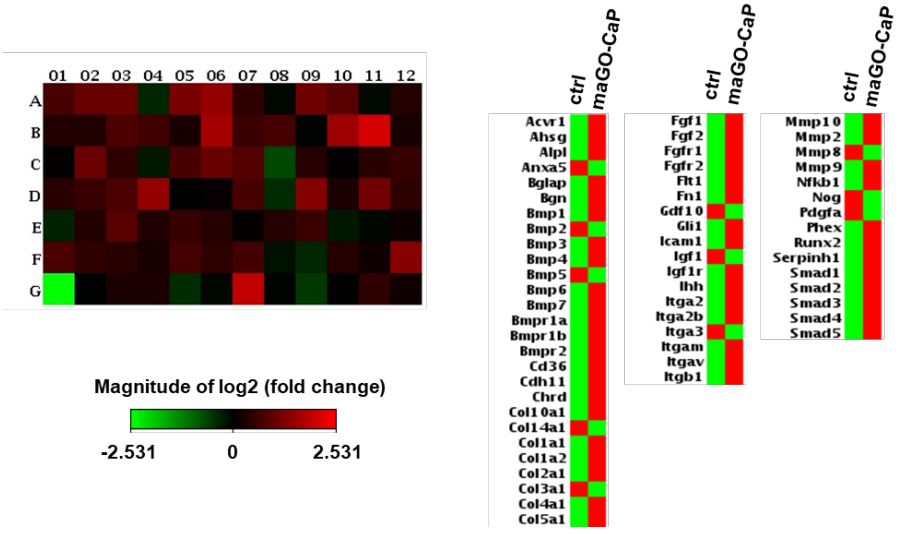

Figure 19. Mice osteogenesis array. Heat-map shows the variation in osteogenic gene expression after one month from injection with maGO-CAP and PBS as control. The experiments were carried out in triplicate and the data were reported as mean. Genes were shown for fold-change variations compared to the controls: red: high expression; green: low expression.

4.4 Conclusions

During the last years, graphene and its derivatives have obtained growing interest as revolutionary candidate carbon-based nanomaterial for biomedical applications. [53] Recently, graphene, particularly in its oxide form, has emerged as a new possible approach to enhance bone regeneration. To date, the majority of the studies on bone have mainly focused on its ability to induce MSCs differentiation into osteoblasts. [5, 7 54] However, none of them took into consideration the key role of immune cell-derived factors in osteoblast differentiation. [55] In this work, we demonstrated that maGO-CaP exerts pro-osteogenic properties, which may partly be mediated *via* monocyte activation, and it is associated with activated BMP and Wnt signaling, two key pathways for osteoblasts. Moreover, the pro-osteogenic potential of maGO-CaP was further validated *in vivo*, showing an increased bone volume fraction due to increased osteoblast activity (**Scheme 1**).

Thus, our results confirm the osteogenic properties of maGO-CaP *in vitro* and show for the first time its osteoblast-supporting effects *in vivo*. Our findings may be important from a public health perspective since they could inspire the use of graphene oxide conjugated with calcium phosphate in implanted constructs or other approaches to support bone regeneration.

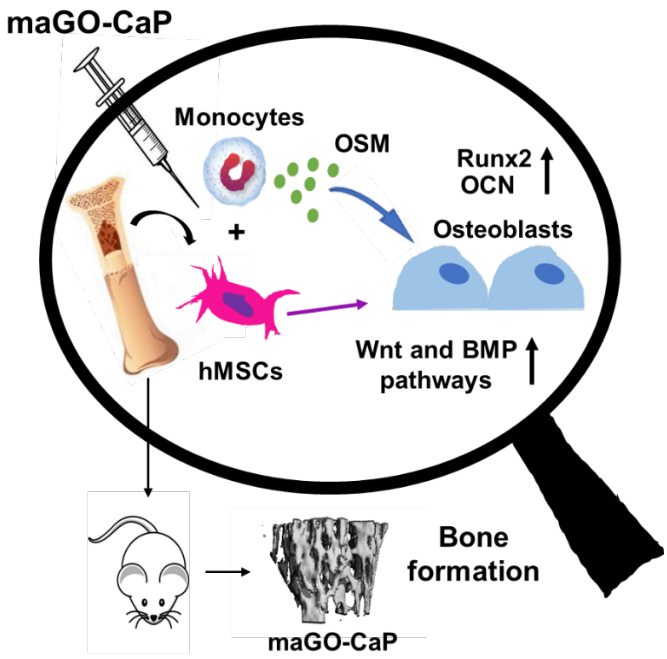

Scheme 1. Schematic diagram showing maGO-CaP function.

4.5 Reference

[1] F. Loi, L. A. Córdova, J. Pajarinen, T. H. Lin, Z. Yao, S. B. Goodman, *Bone*, **2016**, 86, 119.

[2] C. R. Black, V. Goriainov, D. Gibbs, J. Kanczler, R. S. Tare, R. O. Oreffo, *Curr Mol Biol Rep*., **2015**, 1, 132.

[3] N. Dubey, R. Bentini, I. Islam, T. Cao, A. Helio C. Neto, V. Rosa, *Stem cells international* **2015**, 2015, 804213.

[4] R. Tatavarty, H. Ding, G. Lu, R. J. Taylor, X. Bi, *Chem. Commun. (Camb)* **2014**, *50*, 8484.

[5] Y. Talukdar, J.T. Rashkow, G. Lalwani, S. Kanakia, B. Sitharaman, *Biomaterials*, **2014**, 35, 4863.

[6] L. Jin, J. H. Lee, O. S. Jin, Y. C. Shin, M. J. Kim, S. W. Hong, M. H. Lee, J. C. Park, D. W. Han, *J. Nanosci. Nanotechnol.* **2015**, *15*, 7966.

[7] W.C. Lee, C. H. Lim, H. Shi, L. A. Tang, Y. Wang, C. T. Lim, K. P. Loh, *ACS nano* **2011,** *5*, 7334.

[8] O. M. Omar, C. Granéli, K. Ekström, C. Karlsson, A. Johansson, J. Lausmaa, C. L. Wexell, P. Thomsen, *Biomaterials* **2011**, *32*, 8190.

[9] V. Nicolaidou, M. M. Wong, A. N. Redpath, A. Ersek, D.F. Baban, L. M. Williams, A. P. Cope, N. J. Horwood, *PloS one* **2012**, *7*, e39871.

[10] M. Orecchioni, D. A. Jasim, M. Pescatori, R. Manetti, C. Fozza, F. Sgarrella, D. Bedognetti, A. Bianco, K. Kostarelos, L. G. Delogu, *Adv. Healthc. Mater.* **2016**, *5*, 276.

[11] M. W. Pfaffl, *Nucleic. Acids Res*. **2001,** *29*, e45.

[12] M. L. Bouxsein, S. K. Boyd, B. A. Christiansen, R. E. Guldberg, K. J. Jepsen, R. Müller, *J. Bone Miner. Res*., **2010**, 25, 1468.

[13] S. Hengsberger, P. Ammann, B. Legros, R. Rizzoli, P. Zysset, *Bone* **2005**, *36*, 134.

[14] A. Bianco, *Angew. Chem. Int. Ed. Engl*., **2013**, 52, 4986.

[15] M. Orecchioni, D. Bedognetti, F. Sgarrella, F. M. Marincola, A. Bianco, L. G.Delogu, *J. Transl. Med*., **2014**, 12, 138.

[16] T. R. Nayak, H. Andersen, V.S. Makam, C. Khaw, S. Bae, X. Xu, P. L. Ee, J. H. Ahn, B. H. Hong, G. Pastorin, B. Özyilmaz, *ACS Nan,o* **2011**, *5*, 4670.

[17] N. V. Vallabani, S. Mittal, R. K. Shukla, A. K. Pandey, S. R. Dhakate, R. Pasricha, A. Dhawan, *J. Biomed. Nanotechnol.,* **2011**, 7, 106.

[18] S.M. Kang, T. H. Kim, J. W. Choi, *J. Nanosci. Nanotechnol*., **2012**, 7, 5185.

[19] X.F. Zhang, S. Gurunathan, *Int J Nanomedicine,* **2016**, 11, 6635.

[20] G. Y. Chen, D. W. Pang, S. M. Hwang, H. Y. Tuan, Y. C. Hu, *Biomaterials*, **2012**, 33, 418.

[21] J. Qiu, D. Li, X. Mou, J. Li, W. Guo, S. Wang, X. Yu, B. Ma, S. Zhang, W. Tang, Y. Sang P. R. Gil, H. Liu, *Adv. Healthc. Mater*., **2016**, 5, 702.

[22] D. C. Zancanela, A. M. Simão, C. G. Francisco, A. N. de Faria, A. P. Ramos, R. R. Gonçalves, E. Y. Matsubara, J. M. Rosolen, P. Ciancaglini, *J. Mater. Sci. Mater. Med*., **2016**, 27, 71.

[23] J. R. Arron, Y. Choi, Nature, **2000**, 408, 535.

[24] H. Takayanagi, *Nat. Rev. Immunol*., **2007**, 7, 292.

[25] X. Zhi, H. Fang, C. Bao, G. Shen, J. Zhang, K. Wang, S. Guo, T. Wan, D. Cui, *Biomaterials*, **2013**, 34, 5254.

[26] C. Shi, E. G. Pamer, *Nat. Rev. Immunol*., **2011**, 11, 762.

[27] P. Guihard, Y. Danger, B. Brounais, E. David, R. Brion, J. Delecrin, C. D. Richards, S. Chevalier, F. Rédini, D. Heymann, H. Gascan, F. Blanchard, *Stem Cells*, **2012**, 30, 762.

[28] J. L. Millán, M. P. *Whyte Calcif Tissue Int*., **2016**, 98, 398.

[29] S. Jo, J. Han, Y. L. Lee, S. Yoon, J. Lee, S. Wang, T. Kim *Int J Rheum Dis.* **2019**, Int J Rheum, 22, 252

[30] C. Wennberg, L. Hessle, P. Lundberg, S. Mauro, S. Narisawa, U. H. Lerner, J. L. Millán, *J Bone Miner Res.* **2000**, *15*,1879.

[31] N. J. Sheehan, B. M. Slavin, P. R. Kind, J. A. Mathews, *Ann Rheum Dis.* **1983**, *42*, 563.

[32] K. Y. Kang, Y. S. Hong, S. H. Park, J. H. Ju, *Semin Arthritis Rheum*. **2015**, *45*, 202.

[33] S.W. Crowder, D. Prasai, R. Rath, D. A. Balikov, H. Bae, K. Bolotin, H. J. Sung, *Nanoscale*, **2013**, 5, 4171.

[34] J. Li, G. Wang, H. Geng, H. Zhu, M. Zhang, Z. Di, X. Liu, P. K. Chu, X. Wang, *ACS Appl. Mater. Interfaces,* **2015**, 7, 19876.

[35] V. Krishnan, H. U. Bryant, O. A. Macdougald, *J Clin Invest.,* **2006**, 116, 1202.

[36] R.T. Moon, B. Bowerman, M. Boutros, N. Perrimon, *Science*, **2002**, 296, 1644.

[37] P. Duan, L. F. Bonewald, *Int. J. Biochem. Cell Biol*., **2016**, 77, 23.

[38] S. Kishida, H. Yamamoto, S. Ikeda, M. Kishida, I. Sakamoto, S. Koyama, A. Kikuchi, *J Biol Chem.,* **1998**, 273, 10823.

[39] S. Shalini, L. Dorstyn, S. Dawar, S. Kumar *Cell Death Differ.,* **2015**, 22, 526.

[40] L.H. Hoeppner, F. J. Secreto, D. F. Razidlo, T. J. Whitney, J. J. Westendorf, *J Biol Chem*., **2011**, 286, 10950.

[41] E.C. Walker, N.E. McGregor, I.J. Poulton, M. Solano, S. Pompolo, T.J. Fernandes, M.J. Constable, G.C. Nicholson, J.G. Zhang, N.A. Nicola, M.T. Gillespie, T.J. Martin, N.A. Sims, *J Clin Invest.,* **2010**, 120, 582.

[42] H. Y. Song, E. S. Jeon, J. I. Kim, J. S. Jung, J. H. Kim, *J Cell Biochem*., **2007**, 101, 1238.

[43] T. J. Fernandes, J. M. Hodge, P. P. Singh, D. G. Eeles, F. M. Collier, I. Holten, P. R. Ebeling, G. C. Nicholson, J. M. Quinn, *PLoS One*, **2013**, 8, e73266.

[44] P. Guihard, M. A. Boutet, B. Brounais-Le Royer, A. L. Gamblin, J. Amiaud, A. Renaud, M. Berreur, F. Rédini, D. Heymann, P. Layrolle, F. Blanchard, *Am. J. Pathol*., **2015**, 185, 765.

[45] J. Pajarinen, T. Lin, E. Gibon, Y. Kohno, M. Maruyama, K. Nathan, L. Lu, Z. Yao, S. B. Goodman. *Biomaterials,* **2018**, S0142-9612, 30834-7.

[46] K. Takeda, T. Kaisho, S. Akira, *Annu. Rev. Immunol*. **2003**, 21, 335.

[47] J. Ma, R. Liu, X. Wang, Q. Liu, Y. Chen, R. P. Valle, Y. Y. Zuo, T. Xia, S. Liu, *ACS Nano***, 2015**, 9, 10498.

[48] G. Y. Chen, H. J. Yang, C. H. Lu, Y. C. Chao, S. M. Hwang, C. L. Chen, K. W. Lo, L. Y. Sung, W. Y. Luo, H. Y. Tuan, Y. C. Hu, *Biomaterials,* **2012**, 33, 6559.

[49] G. Qu, S. Liu, S. Zhang, L. Wang, X. Wang, B. Sun, N. Yin, X. Gao, T. Xia, J. J. Chen, G. B. Jiang, *ACS Nano*, **2013**, 7, 5732.

[50] J. Russier, V. León, M. Orecchioni, E. Hirata, P. Virdis, C. Fozza, F. Sgarrella, G. Cuniberti, M. Prato, E. Vázquez, A. Bianco, L. G. Delogu, *Angew. Chem. Int. Ed. Engl*. **2017**, *56*, 3014.

[51] S. P. Kastl, W. S. Speidl, C. Kaun, K. M. Katsaros, G. Rega, T. Afonyushkin, V. N. Bochkov, P. Valent, A. Assadian, G. W. Hagmueller, M. Hoeth, R. de Martin, Y. Ma, G. Maurer, K. Huber, *J. Wojta Arterioscler Thromb Vasc Biol.*, **2008**, 28, 498.

[52] S. P. Kastl, W. S. Speidl, K. M. Katsaros, C. Kaun, G. Rega, A. Assadian, G. W. Hagmueller, M. Hoeth, R. de Martin, Y. Ma, G. Maurer, K. Huber, J. Wojta, *Blood*, **2009**, 114,2812.

[53] K.V. Krishna, C. Menard-Moyon, S. Verma, A. Bianco, *Nanomedicine*, 2013, 8, 1669.

[54] L. Jin, J.H. Lee, O.S. Jin, Y. C. Shin, M. J. Kim, S. W. Hong, M. H. Lee, J. Park, D. W. Han, *Journal of Nanoscience and Nanotechnology,* **2015**, 15, 7966.

[55] E. Hirata, E. Miyako, N. Hanagata, N. Ushijima, N. Sakaguchi, J. Russier, M. Yudasaka, S. Iijima, A. Bianco, A. Yokoyamaa, *Nanoscale*, **2016**, 8, 14514.

5. Silver nanoparticles and cancer treatment

5.1 Introduction

Cancer is the second commonest cause of death in the world. Worldwide cancer incidence and mortality are rapidly increasing. In 2018, cancer was responsible for approximately 9.6 million deaths and 18.1 million of new cancer cases. [1] The therapeutic treatment of cancer is usually a combination of surgery and/or radiotherapy with chemotherapy. The problems of these current treatments are the severe side effects that may develop. [2] Chemotherapy agents can lead to common complications including clinical systemic toxicity and development of resistance. Over the past few years, a new research field is rising: cancer nanomedicine. Cancer nanomedicine aims to develop new nanosystems with potential applications for early detection, accurate diagnosis and personalized treatment of cancer. [3, 4] Particles in nano-size can offer peculiar interactions with the biomolecules, present on the surface or inside the cells, leading to a revolution in cancer diagnosis and treatment. Various nanoparticles have been recently studied in cancer research, including carbon nanotubes, [5] paramagnetic nanoparticles, [6] liposomes, [7] gold nanoparticles [8] and many others. [9] Among the commonly used nanoparticles, silver nanoparticles (AgNPs) show interesting physical-chemical features. Silver is a noble metal with well-known anti-bacterial properties and low toxicity. Moreover, an increasing number of silver compounds were found to be active against several types of cancer cells, but only *in vitro*. [10] Indeed, the very effective physiological mechanisms of detoxification are able to reduce the bioavailability of silver in the body. To avoid this problem, AgNPs can be considered an excellent solution. AgNPs can be internalized by cells via endocytosis and, subsequentially, release Ag^+ ions at specific target sites. [11] Recent evidence suggests that AgNPs induce cytotoxicity stimulating the production of reactive oxygen species. [12, 13] Anyway, further investigations have to be carried out to elucidate other mechanisms involved in AgNPs biological activity.

There are several ways to synthesize AgNPs, but the most employed during the last few years is the biosynthesis from plants, bacteria, and fungi extracts. [14] This approach is easy, cheap and eco-friendly. The biosynthesis is simply performed by adding a silver salt, usually silver nitrate ($AgNO_3$), to plant extracts. At this point, the biomolecules of such extracts present in solution, including terpenoids, polyphenols, enzymes, proteins, are able to reduce silver ions to metal nanoparticles. The origin of the extracts, the temperature and pH of the solution and the ratio between extracts and

$AgNO_3$ influence the shape and dimensions of nanoparticles, which in turn affect the biological responses of AgNPs. [15, 16] Moreover, the presence of biomolecules in the reaction medium, especially proteins and enzymes, produce what is called as "capping". The capping is a layer of biomolecules present on the surface of the particles, which determinates behavioral changes of AgNPs. Several studies suggest that "capped" nanoparticles are more biocompatible, less cytotoxic but, at the same time, more efficient compared to "naked" nanoparticles. [17, 18]

Following these evidences, we prepared AgNPs from the extracts of *Artemisia arborescens*. *Artemisia arborescens* is a typical Mediterranean plant very common in Sardinia (Italy). This plant, like some others of the genus *Artemisia*, provides essential oils used historically in folk medicine to treat inflammations and other states of health. The *Artemisa arborescens* pharmacological properties are under investigation for several medical purposes. [19]

To evaluate any possible differences in the biological features, three different *Artemisia*-AgNPs were prepared using three different pH values (7, 8 and 9) during the biosynthesis process. The variation of pH determinates a change of their size and influences the capping formation on their surface.

The *Artemisia*-AgNPs were fully characterized and their effects were tested on cancer cell lines, in particular HeLa and MCF-7. We found a strong cytotoxic action of *Artemisia*-AgNPs synthesized at pH 7, compared to the others, with dose-dependent growth inhibition of cancer cells after 24 hours and 48 hours of treatment. Based on these results, we evaluated the impact on cell cycle, observing a G1 arrest mediated by *Artemisia*-AgNPs. The apoptosis action of *Artemisia*-AgNPs was demonstrated by flow cytometry using Annexin V/7aad labeling. The clonogenic assay, instead, was used to evaluate the capacity of producing progeny after treatment. The complete lack of cell colonies after treatment demonstrated cell reproducibility death. Furthermore, to have a wide overview on the biological activity of *Artemisia*-AgNPs, we performed RNA-sequencing obtaining exciting information on *Artemisia*-AgNPs action. These preliminary data suggest the potentiality of *Artemisia*-AgNPs as a good candidate anticancer agent and pave the way for further analysis in cancer research.

5.2 Materials and methods

5.2.1 *Artemisa*-AgNPs synthesis and characterization

The biosynthetic procedure was carried out by extracting *Artemisia* leaves in hydroalcoholic solutions and using such extracts to reduce silver nitrate (2 mmol) at room temperature by changing the pH of the solutions. The reaction was completed within 24 hours (catalyzed reduction). AgNPs were then recovered by ultracentrifugation. AgNPs were prepared at three different pH values (7, 8, 9).

5.2.2 Cell cultures

HeLa (cervix adenocarcinoma), MCF-7 (breast cancer) and PC3 (prostate cancer) were purchased from ATCC. Cells were cultured in Dulbecco's Modified Eagle's Medium (Gibco), containing 1% of penicillin/streptomycin solution and 10% fetal bovine solution (FBS) (Gibco). All cell lines were grown at 37 °C in 5% CO_2 in a humidified incubator.

5.2.3 Proliferation assay (XTT)

Cell viability was analyzed using the XTT assay (Cell Proliferation Kit II, Roche). Each cell line was seeded in 96-well plates at a density between 1500 and 2000 cells/well, considering the different size, phenotype, and cellular duplication. After that, cells were treated with increasing concentrations (from 0.5 to 20 µg/ml) of three different *Artemisia*-AgNPs (synthesized at 7, 8 and 9 pH) or left untreated. After 24 hours and 48 hours of treatment, XTT assay was performed. The assay is based on the conversion of the tetrazolium salt XTT, in the presence of an electron-coupling reagent, to formazan salt. A mix containing 0.5 µL of XTT electron coupling reagent, 25 µL of labeling reagent and 74,5 µL of medium, for a final volume of 100 µL/well, was prepared. Cells were incubated with this mix for four hours at 37°C. Following incubation time, the absorbance was measured at 490nm using a spectrophotometric plate reader. All experiments were carried out in triplicate.

5.2.4 Cell cycle analysis

HeLa and MCF-7 were seeded in 6-well plates at the concentration of 500.000 cell/well. After 24 hours, cells were treated or not treated with 7 µg/ml of *Artemisia*-AgNPs pH7 for ~~6~~ six hours and 18 hours. After incubation times, supernatants and adherent cells were collected. Cells were then centrifuged at 500 g for five minutes. Thus, the pellets were washed with PBS and centrifugate again at the same conditions as before. At this point, pellets were resuspended in 200 µl of PBS and fixed in 70% ice-cold ethanol in agitation using a vortex. The samples were preserved at -20ºC for a time between one and seven days. Fixed cells were washed twice with PBS, resuspended in 200 µl of PBS and incubated with 20 µl of 7aad label for 20 minutes under dark conditions. The cell cycle was evaluated using FACS CANTO II (BD Biosciences) by collecting 20.000 events. The data were analyzed using DIVA software (BD Biosciences).

5.2.5 Necrosis and apoptosis evaluation

The apoptosis assay was performed using Annexin V/7aad labeling. Briefly, HeLa and MCF-7 were treated with 7µg/ml of *Artemisia*-AgNPs for 24 hours or left untreated. The supernatants and adherent cells were collected and washed with PBS. The pellets were resuspended in 50 µl of Annexin V 1× buffer and stained with Annexin V/7aad. Cells were incubated for 20 minutes in the dark. After incubation time, 200 µl of Annexin V 1× buffer was added in each sample and the cell fluorescence was measured by flow cytometry (FACS CANTO II BD Biosciences), collecting 20.000 events. DIVA software was used to analyze the data.

5.2.6 Colony assay

To evaluate cell colony formation, 100-200 cells/well were seeded in 6-well plates. After five-seven days, when cells started to form colonies were treated with 7 µg/ml of *Artemisia*-AgNPs pH7 or left

untreated. Cells were incubated at 37°C and maintained in culture for two weeks until control samples had formed enough visible colonies. The medium, with or without AgNPs, was changed every three days. To visualize cell colonies, the cells were stained with 2 mL of 6.0% glutaraldehyde and 0.5% crystal violet for 30 minutes. After washing with ddH_20, the stained colonies were counted and treated samples were compared with the controls.

5.2.7 mRNA extraction and preparation of mRNA-seq library

HeLa cells were seeded in 6-well plates ($2x10^5$) and treated with 7µg/ml of *Artemisia*-AgNPs for six hours and 18 hours or left untreated. After incubation time, cells were collected by centrifugation at 500 g for five minutes. The pellets were washed twice with PBS and centrifuged at the same conditions. Total RNA was extracted using RNeasy MINI Kit (Qiagen) following manufacturer's protocol. The RNA quality was assessed by Agilent 2100 Bioanalyzer. The rRNA was removed from total RNA using RNaseH digestion and ribosomal-depleted RNA was purified by VAHTSTM RNA Clean Beads.

cDNA synthesis was performed using random primers, incorporating dUTP to label the second strand. After magnetic bead purification, fragments of 150-200 bp were obtained. The libraries were sequenced on the Hiseq-PE150.

5.2.8 Quality Control and Gene Analysis

Firstly, the raw obtained were checked in terms of quality with fastqc. To filter the low-quality and unmeasured bases, we used trimmomatic in order to achieve final clean data. To provide the reference of genome and gene annotation files, we downloaded the hg38 reference genome (grch38.p12. genome) and gene annotation GTF (GRCh38, version 30, Ensembl 96) in gencode database. We used RSEM software to quantify the transcript abundances from RNA-Seq data. The index was established by STAR in order to extract by RSEM the sequence of each transcript from the reference genome sequence through the gene annotation files. To achieve gene expression results from samples, STAR

alignment and expression level analysis of clean reads, obtained by RSEM, were performed. The number of readings segments that mapped to each gene sequence is calculated by FPKM (fragments per kilobases per million reads), considering the gene length and the sequencing depth. FPKM is a normalized estimator which allows to estimate the expression value of a gene. To analyze the difference in gene expression between control group and treated samples, DEseq was performed. The differential gene screening criteria were based on the parameter values log2 fold-change and p-value ($|logFC| \geq 2$ and p-value < 0.05).

5.2.9 GO Enrichment and KEGG Pathway Analysis

Since the functional and pathway enrichment analysis of differentially expressed genes (DEGs) was needed in order to clarify the biological processes and molecular mechanisms , GO enrichment and KEGG pathway analysis were applied for the identification of key genes and pathways involved. GO stands for Gene Ontology database, which is an international classification system standardized for gene functions. The classification of genes is organized in ontologies (or graph structures), which are grouped into three categories: molecular function, cellular component and biological process. Gene Ontology database is usually used for annotating sequencing and gene products. Therefore, GO functional analysis offers the possibility to provide a GO functional classification and GO function significance enrichment of DEGs. Using GO significant enrichment analysis, the major biological functions of DEGs were determined. [20]

KEGG (Kyoto Encyclopedia of Genes and Genomes) is a database for systematic analysis of genome information and gene function. The KEGG database allows the analysis of the metabolic pathways and functions of genes products, facilitating the investigation of genes and gene expression networks. KEGG incorporates data from genome, chemical molecules and biochemical systems, including metabolic pathways, drugs, diseases and gene sequences. KEGG analysis was performed to evaluate the pathway significance enrichment and the hypergeometric test was used to find out the pathway significantly enriched in the DEGs compared with the whole genome background. [21]

5.2.10 Key modules and hub genes identification

To evaluate the hub genes, we performed gene network analysis using STRING (http://string-db.org). STRING contains a database able to predict and verify protein-protein interactions, including direct physical interactions and indirect functional relationships. STRING is based on the use of experimental data from content management literature and bioinformatic methods to predicts results. The biological methods employed for the analysis include chromosome proximity, gene fusion, phylogenetic tree and gene co-expression of gene chip data. A scoring mechanism is used by the system to set the results obtained by different methods. STRING enables to construct an interaction network combining the results of differential expression analysis with the interactions between the databases and the DEGs.

5.3 Results and discussion

5.3.1 Synthesis and cytotoxic effects of *Artemisia*-AgNPs on cancer cell lines

Artemisia extracts were used to reduce silver nitrate to AgNPs. The biosynthesis procedure was carried out at three different pH, from 7 to 9, obtained three types of *Artemisia*-AgNPs different for size and capping. The average size of each *Artemisia*-AgNPs is the following: 29,33 nm for pH 7, 14,60 nm for pH 8 and 3,61 for pH 9. Electron microscopy (TEM) shows nearly spherical nanoparticles with an average size smaller than 20nm, as confirmed also by dynamic light scattering (**Figure 1A and B**).

The UV-vis spectra show a typical peak due to plasmon resonance around 420 nm, in agreement with the presence of spherical particles, for the *Artemisia*-AgNPs pH 7, 8 e 9. In **Figure 2A** is reported the UV-vis spectrum of *Artemisia*-AgNPs pH 7 as an example. FTIR analysis evidences bands relative to the stretching of OH, NH and C=O groups, confirming the presence of surface capping (**Figure 2B**).

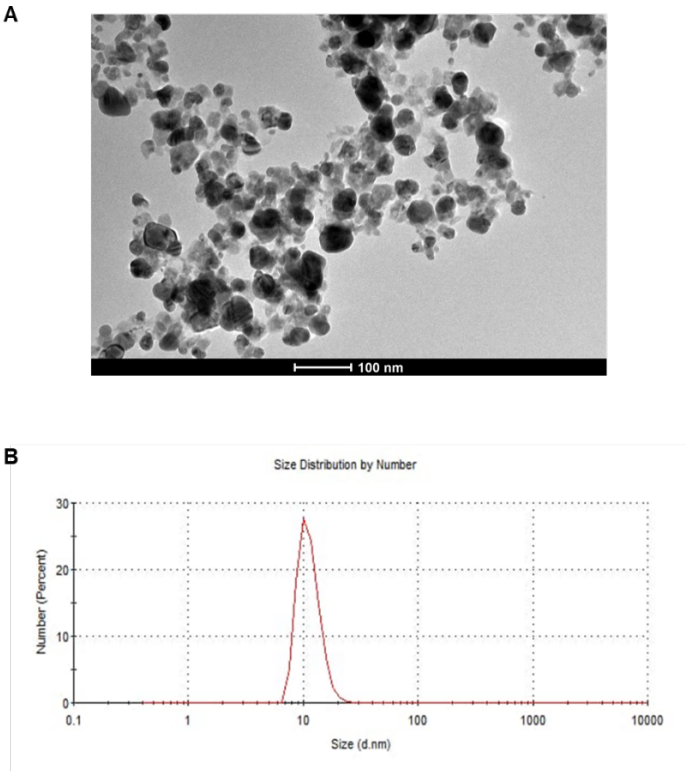

Figure 1. A) TEM image and B) dynamic light scattering.

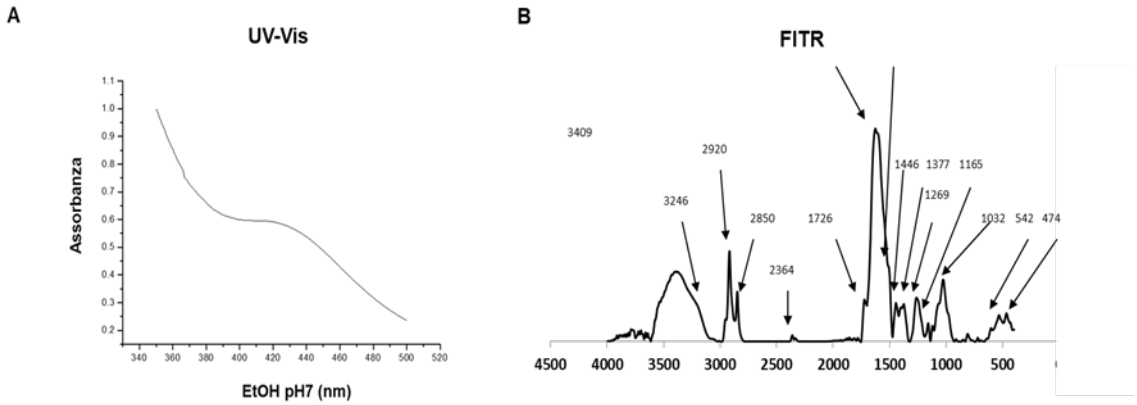

Figure 2. UV-vis and FTIR spectra. A) UV-vis spectrum of *Artemisia*-AgNPs solution at pH 7. B) FTIR analysis show the surface plasmon resonance of *Artemisia*-AgNPs pH 7.

Firstly, we evaluated the antiproliferative effects of the three types of *Artemisia*-AgNPs (pH 7, pH 8 and pH 9) on three different cell cancer lines (HeLa, MCF-7 and PC3). The cells were treated with increasing concentration of each *Artemisia*-AgNPs, from 0.5 to 20µg/ml. To analyze cell viability, XTT assay was performed. As shown in **Figure 3**, the *Artemisia*-AgNPs pH7 revealed a higher antiproliferative action compared to the others, with a decrease of cell viability correlated to the dose used. Several studies demonstrated the ability of AgNPs to exhibit cell proliferation inhibition, inducing cell death. [22, 23, 24] Moreover, it was shown that the size and surface area of AgNPS are able to influence the cytotoxicity effect. [25, 26] According to our results, recent evidences suggest that the appropriate size for cellular uptake in order to achieve the greatest biological activity of nanoparticles without the risk of haemolysis is around 40-50 nm. [27, 28]

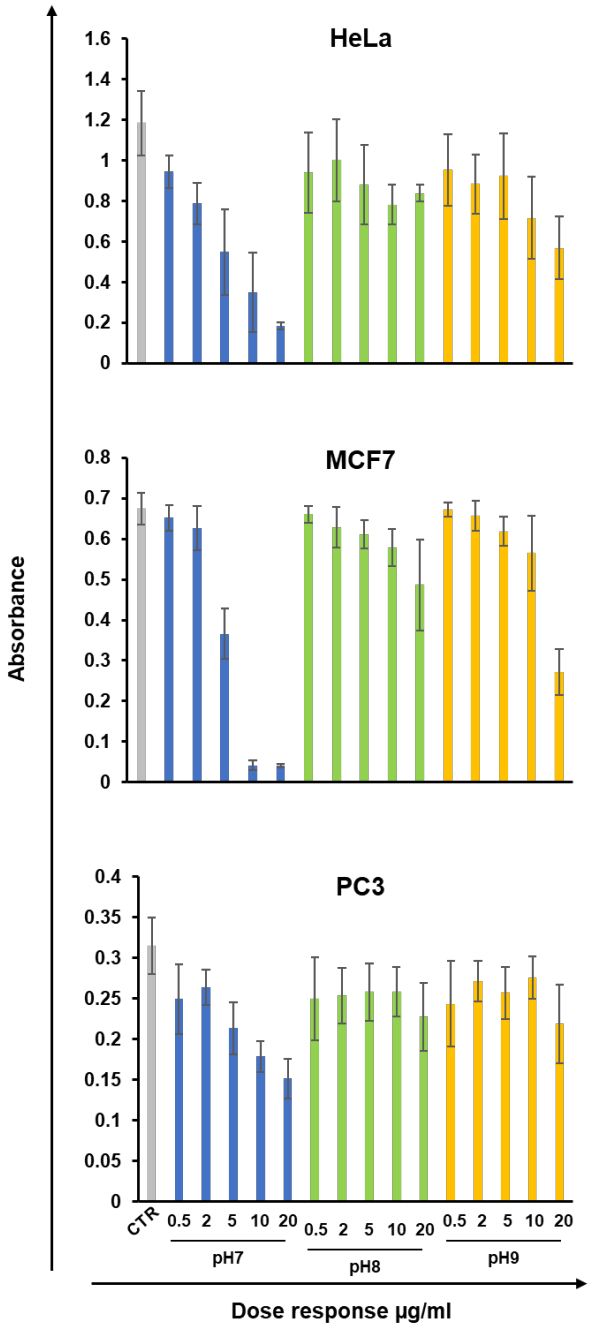

Figure 3. XTT assay. HeLa, MCF-7 and PC3 were treated with increasing doses (0.5-20 µg/ml) of each *Artemisia*-AgNPs (pH 7, pH 8 and pH 9). XTT assay was performed to evaluate cell viability.

Moreover, XTT analysis shows a more evident effect of *Artemisia*-AgNPs pH7 on HeLa and, especially, MCF-7 compared to PC3 (**Figure 3**). In line with our results, Sadegh *et al*. described more selective effects of green synthesized AgNPs against MCF-7 cell line. [29]

Based on these data, we decided to focus only on *Artemisia*-AgNPs pH7 and evaluate their specific effects on HeLa and MCF-7. Therefore, we repeated the XTT assay at 24 hours and 48 hours, using concentrations of 2, 5 and 10 µg/ml of *Artemisia*-AgNPs pH 7 (**Figure 4**).

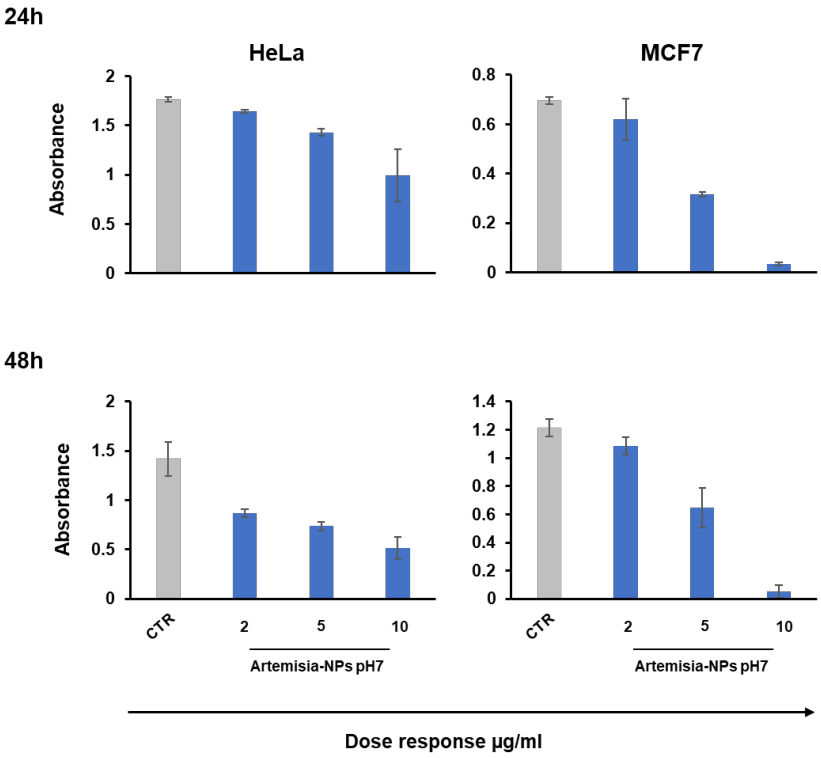

Figure 4. XTT assay of *Artemisia*-AgNPs pH7 on HeLa and MCF-7. HeLa and MCF-7 were cultured with 2, 5 and 10 µg/ml of *Artemisia*-AgNPs pH 7. Cell viability was evaluated using XTT assay.

We found a strong antiproliferative effect on HeLa and MCF-7 notable at the concentration between 5 and 10µg/ml of *Artemisia*-AgNPs pH7 (**Figure 4**). Hence, 7µg/ml of *Artemisia*-AgNPs pH7 was considered to be the best dose able to reduce significantly the cell viability. **Figure 5** shows the images of HeLa and MCF-7 after 24 hours of treatment with 7µg/ml of *Artemisia*-AgNPs pH7. Indeed, compared to control, after 24 hours of treatment, most cells appear clearly suffering, detached from the plate and dead.

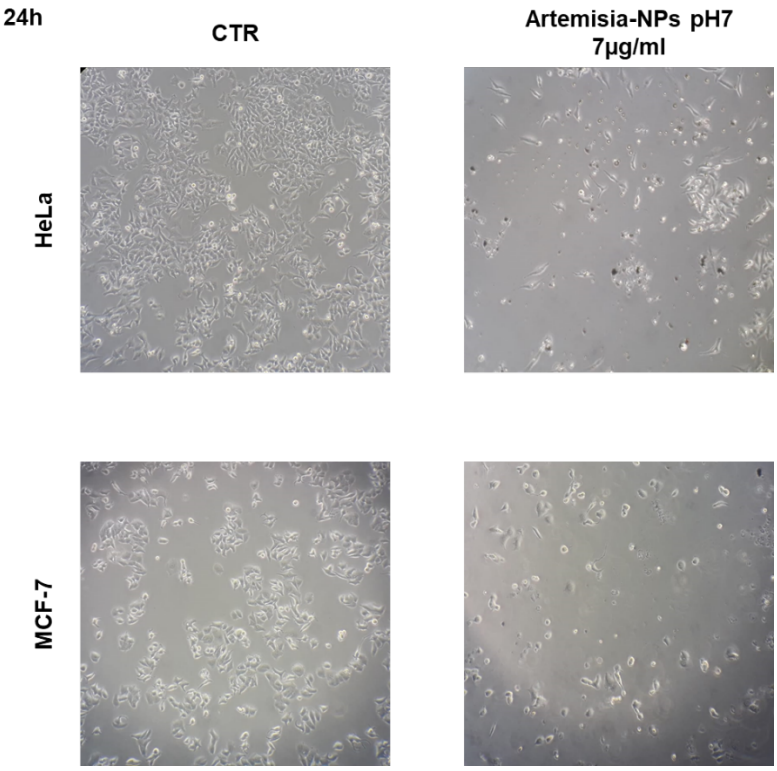

Figure 5. Microscope images of HeLa and MCF-7 treated with 7 µg/ml of *Artemisia*-AgNPs pH 7.

5.3.2 Cell cycle impact

To evaluate the impact on cell cycle, we treated HeLa and MCF-7 for six hours and 18 hours with 7 µg/ml of *Artemisia*-AgNPs pH 7. Surprisingly, already after six hours of treatment, we observed a reduction of the number of HeLa cells in G2/M phase compared to control samples (**Figure 6**). At 18 hours of incubation, the majority of cells were in the G0/G1 phase, with a strong decrease of G2/M phase and an increase of SubG1 phase, index of cellular death. (**Figure 6**). Similar results were found in *Artemisia*-AgNPs-treated MCF-7 (**Figure 7**). After 18 hours of incubation, the arrest of cells in G0/G1 phase was significant, with a considerable increase of SubG1 phase (**Figure 7**). Other studies evaluated the cell cycle of cancer cell lines after treatment with AgNPs. HeLa cells exposed to 10–50 µg/ml concentrations of AgNPs for 24 hours showed a relevant increase of the SubG1 population

and cells were not able to go through G2 checkpoint. [30] Contrary to our results, other authors observed that AgNPs induced accumulation of G2/M-phase cells accompanied by a decrease in G1 population in lung epithelial cells and glioblastoma cells. [31, 32] The divergence in cell cycle data may be due to both different cell lines and distinct AgNPs used for the studies. Moreover, the capping on AgNPs, consisting of several proteins and enzymes, could influence the cell cycle of cancerous cells. The biomolecules released by *Artemisia arborescens* extracts during AgNPs synthesis process may assemble a peculiar capping with active agents able to improve the biological behaviors of AgNPs. Anyway, further investigations are needed to better understand the antiproliferative mechanisms of AgNPs.

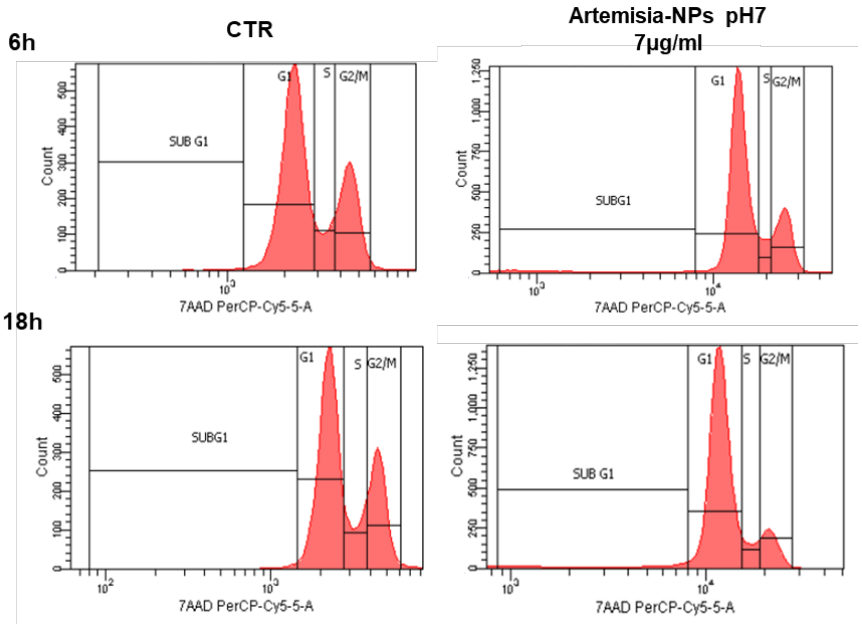

Figure 6. Cell cycle HeLa. HeLa cells were treated with 7 µg/ml of *Artemisia*-AgNPs pH 7 or left untreated. Cell cycle was evaluated after six hours and 18 hours by flow cytometry.

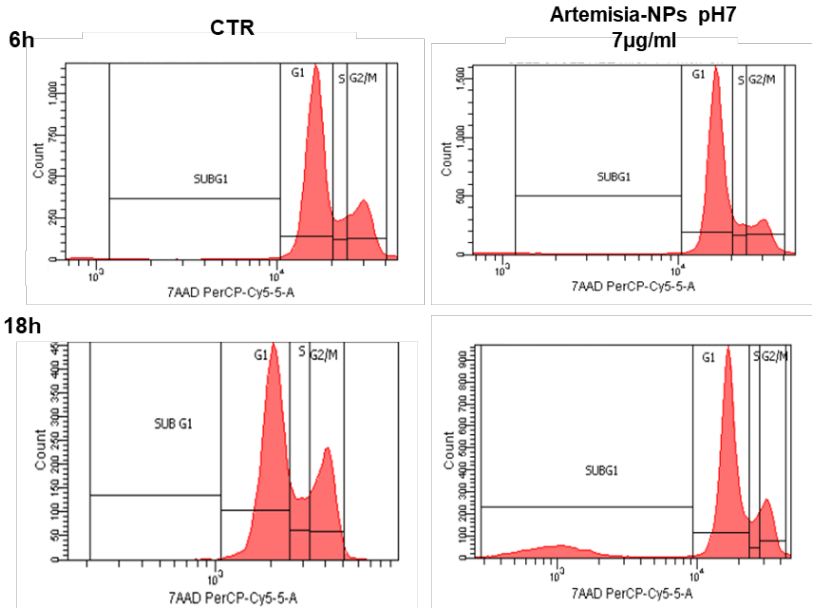

Figure 7. Cell cycle MCF-7. MCF-7 cells were treated with 7 µg/ml of *Artemisia*-AgNPs pH 7 or left untreated. Cell cycle was evaluated after six hours and 18 hours by flow cytometry.

5.3.3 *Artemisia*-AgNPs induce apoptosis and inhibit colony formation in cancer cells

To discriminate the type of cell death induced by *Artemisia*-AgNPs pH7, Annexin V/7aad assay was performed. Cells were incubated with 7µg/ml of *Artemisia*-AgNPs pH7 for 24 hours in order to ensure a significant number of dead cells. As shown in **Figure 8**, *Artemisia*-AgNPs induced significant apoptotic effects in both cell lines. Furthermore, compared to control, a slight increment of necrotic cells was noticed (**Figure 8**). Several studies demonstrated the apoptotic effects of AgNPs on various cell lines. [33, 34, 35, 36] The mode of cytotoxicity may be due to different concentrations used, since, at higher doses, the necrotic effects became more prevalent. [37]

Moreover, we evaluated the ability of *Artemisia*-AgNPs pH7 to arrest the cell colonies formation. The number of colonies formed after two weeks of *Artemisia*-AgNPs pH7 exposure was determined

using a clonogenic assay. Clonal growth was inhibited by 7µg/ml of *Artemisia*-AgNPs pH7 as shown in **Figure 9**.

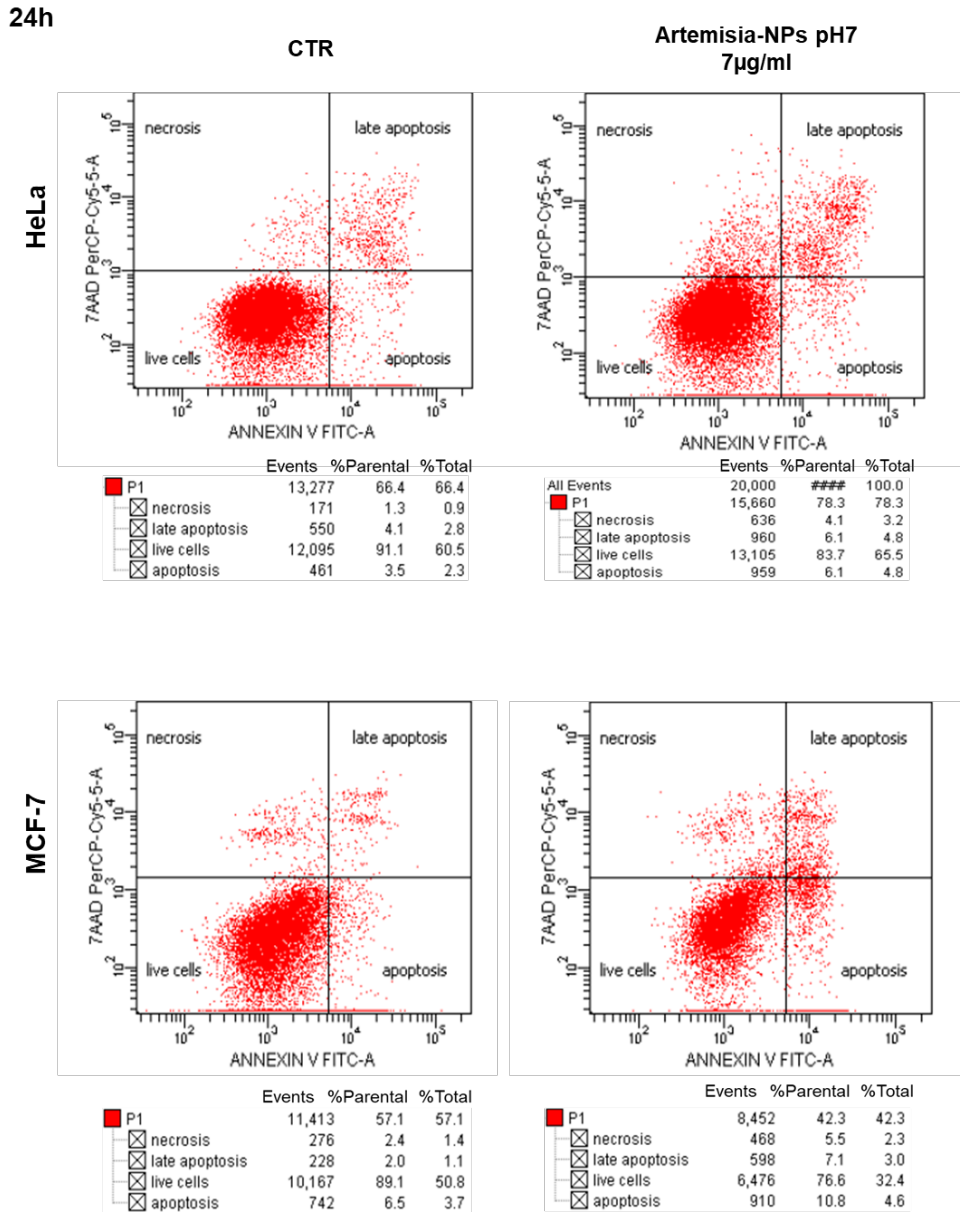

Figure 8. Apoptosis/Necrosis assay. On the left control samples, while on the rights samples treated with 7 µg/ml of *Artemisia*-AgNPs pH 7. Above HeLa cells and below MCF-7 cells. Cells were stained with Annexin V/7aad and analyzed by flow cytometry.

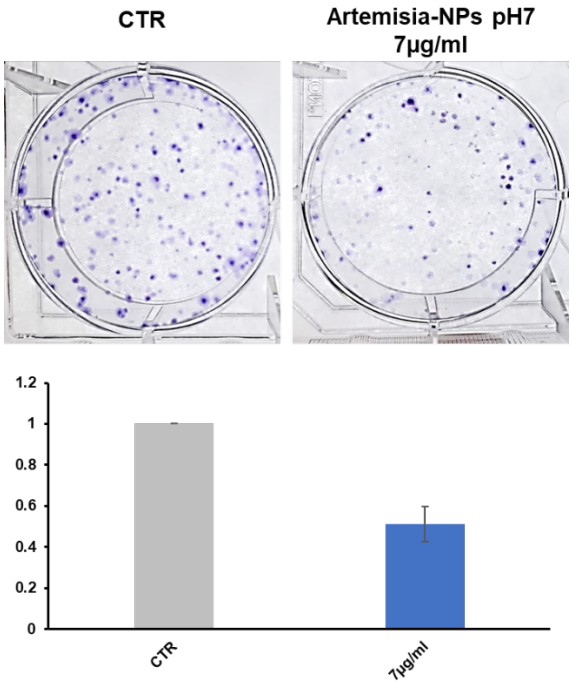

Figure 9. Clonogenic assay. After the formation of the first colonies, cells were treated with 7 µg/ml of *Artemisia*-AgNPs pH 7. Cell colonies were stained and counted.

5.3.4 *Artemisia*-AgNPs impact on gene expression

To have a wide overview on the impact of *Artemisia*-AgNPs on gene expression, we performed RNA-sequencing on HeLa cells, in collaboration with the Shantou University. Applying the parameter values log2 fold-change and p-value as reference indicators for significant difference, we found several differentially expressed genes (DEGs) after six hours and 18 hours of *Artemisia*-AgNPs treatment (**Figure 10**). In detail, we found 2286 up-regulated and 328 down-regulated genes after six hours of treatment; while after 18 hours of treatment 2080 up-regulated and 316 down-regulated genes were detected (**Figure 11**).

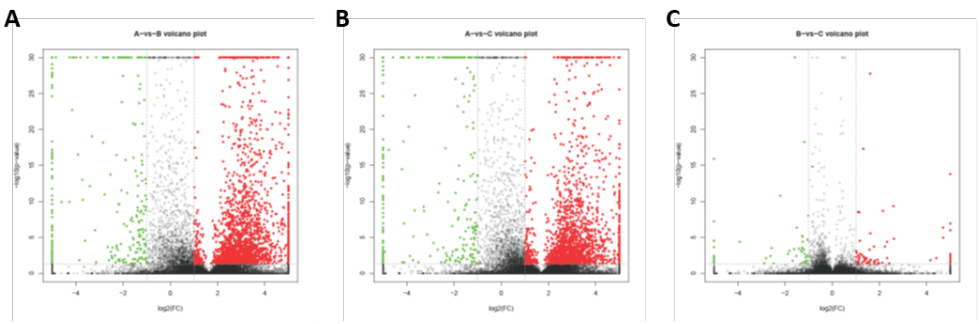

Figure 10. Volcanic map of differential genes. The DEGs set after six hours and 18 hours of *Artemisia*-AgNPs treatment. Red dots indicate up-regulated genes, green dots represent down-regulated genes and black dots indicate genes with no significant difference. (|logFC| ≥ 2 and p value < 0.05). A: CTR VS 6h; B: CTR VS 12h; C: CTR VS 18h.

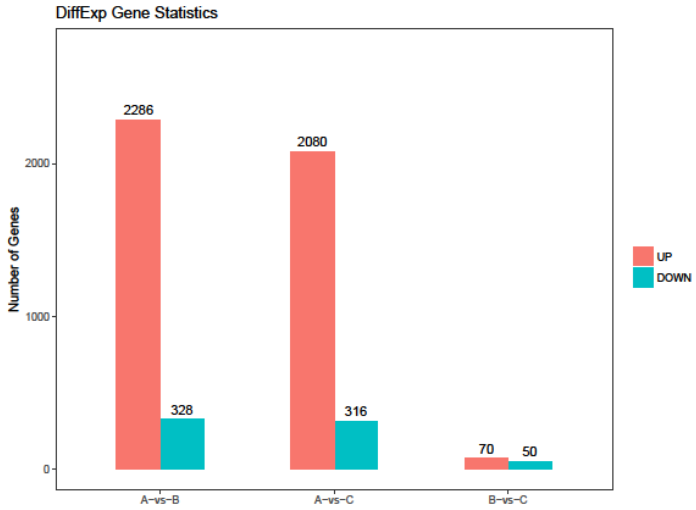

Figure 11. Histogram of differential genes. The DEGs set disturbed by *Artemisia*-AgNPs treatment (|logFC| ≥ 2 and Pvalue < 0.05).

To evaluate the functions of the differential expressed genes, gene ontology (GO) was carried out using online software (OmicShare tools). This tool enables to analyze the cellular components correlated to DEGs. *Artemisia*-AgNPs appear to work at intracellular level, with enriched genes mainly expressed in organelle part and their membranes (**Figure 12**).

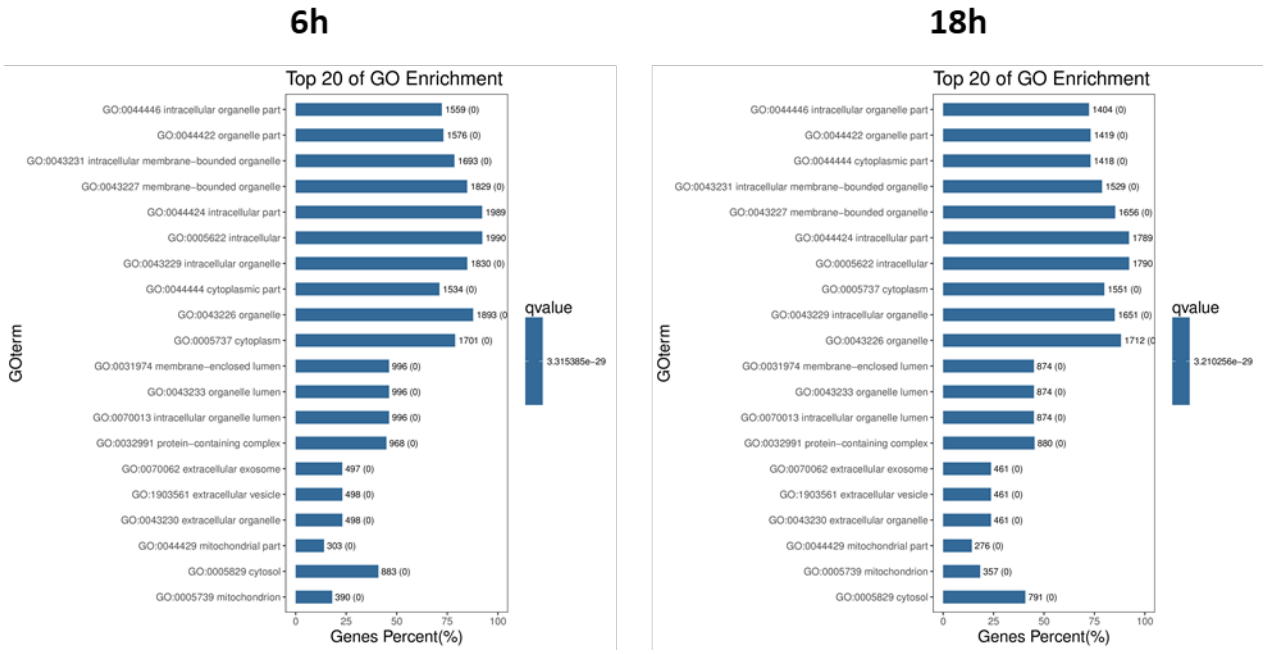

Figure 12. Go enrichment. The functions of the different expressed genes were analyzed using Go enrichment.

Moreover, KEGG pathway analysis was performed to further characterize the differentially expressed genes, investigating the metabolic and signal transduction pathways involved. After *Artemisia*-AgNPs treatment, compared to control, the DEGs were correlated to metabolism pathways in general, but also to signal transduction and cell growth and death (**Figure 13**). Regarding human diseases, the KEGG analysis showed DEGs mainly enriched in infections and cancers (**Figure 13**).

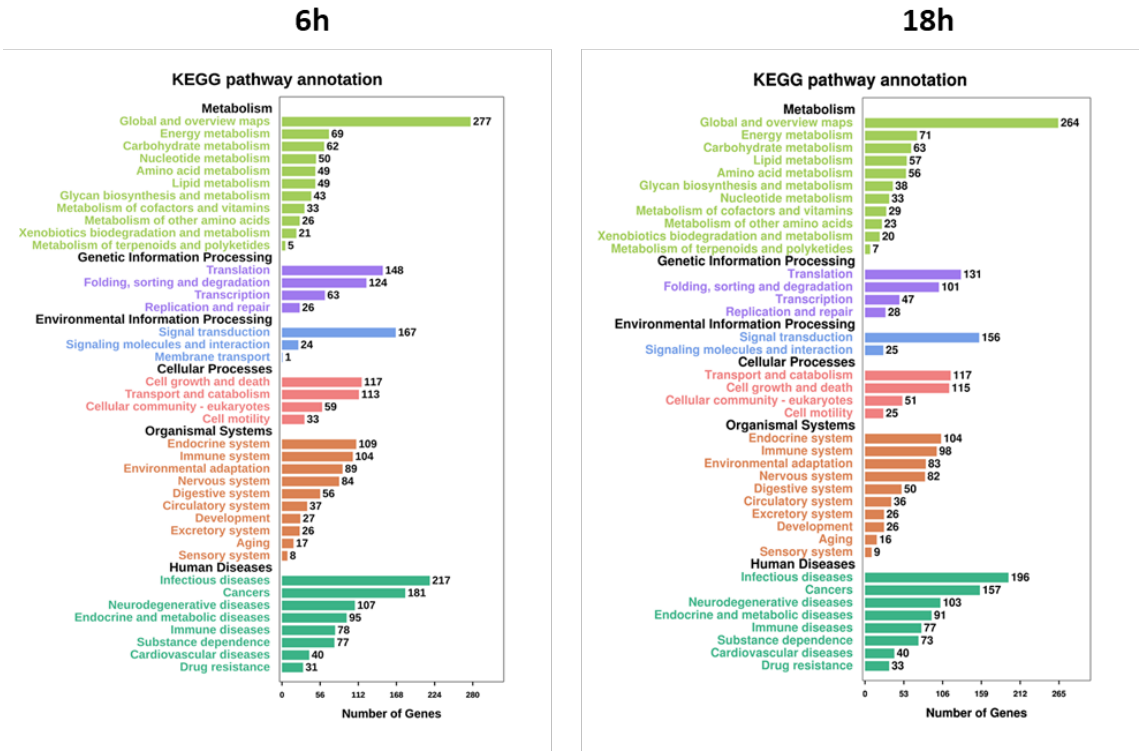

Figure 13. KEGG analysis. The pathways involved in the DEGs were analyzed using KEGG analysis.

We selected p53 pathway, as one of the most important pathways involved in carcinogenesis, and we analyzed the DEGs using KEGG. As shown in **Figure 14**, p53 is over-expressed following the *Artemisia*-AgNPs treatment compared to the control sample. Other authors showed the involvement of p53 and the critical role of p53 upregulation in AgNP-mediated cell death in cancer cell lines. [38, 39] Moreover, p21, a major target of p53 activity associated with DNA damage and G1 cell cycle arrest, was found to be up-regulated after *Artemisia*-AgNPs. Furthermore, Bax gene, a member of the Bcl-2 gene family involved in p53-mediated apoptosis, was found to be up-regulated by *Artemisia*-AgNPs treatment. These outcomes are in line with the results described before regarding cell cycle and apoptosis.

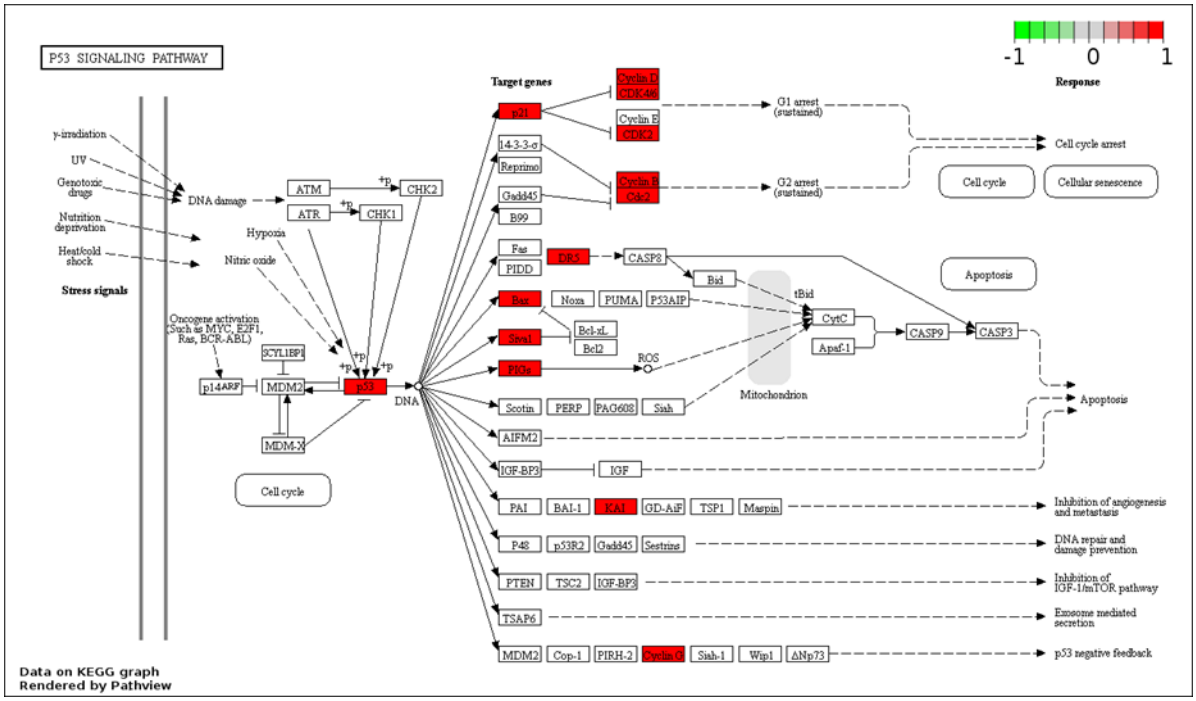

Figure 14. P53 pathway. P53 pathway was investigated using KEGG analysis.

Moreover, we evaluated the protein-protein interaction network using an online mapping tool (NetworkAnalyst3.0) (**Figure 15**). From the PPI network analysis, we evaluated the top 15 genes classified as hub genes by the degree. Following the name of the hub genes: UBC, UBA52, RPS27A, RPS3, FAU, RPL7, RPL23A, RPL4, RPLP0, RPS5, RPL9, RPS14, RPS2, RPL3, RPL23.

Therefore, we analyzed the protein-protein interactions of hub genes (**Figure 16**).

The results of functional and pathway enrichment analysis showed that these 15 hub genes were involved in several biological processes, including regulation of gene expression, DNA damage response, genome nucleotide-excision repair and ribosome (**Table1**).

Anyway, further evaluations have to be performed in order to validate the RNA sequencing data.

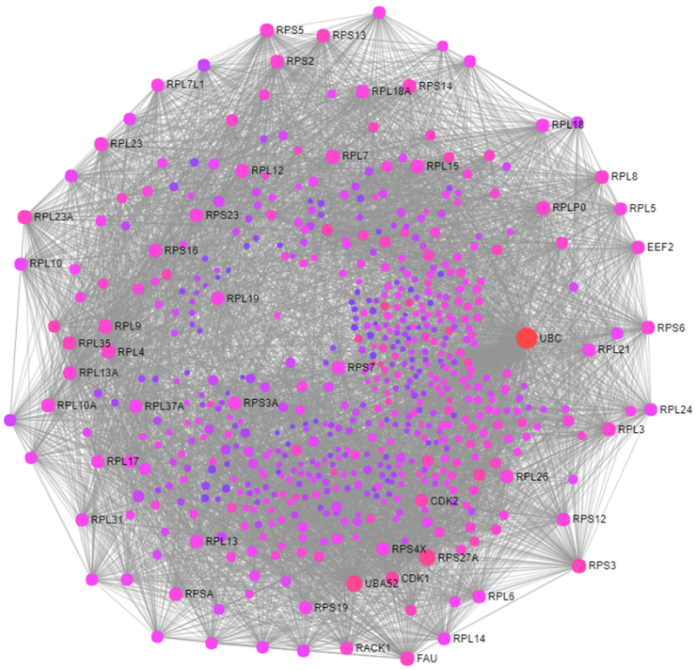

Figure 15. The PPI interaction network of DEGs. The nodes represent the differential genes and the connections between the nodes reveal the interactions between the genes. The size of the nodes indicates the degree of the genes and the different colors point the distinct gene expression (in red are up-regulated genes and in violet those less up-regulated).

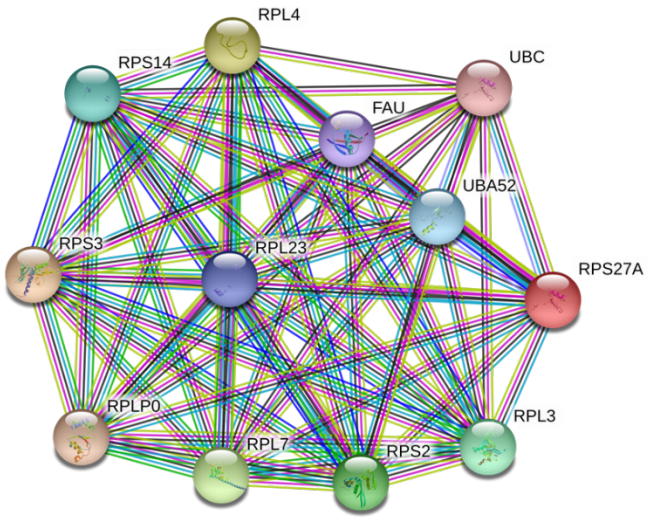

Figure 16. The PPI interaction network of hub genes. Co-expression network with top hub DEGs.

Category	Term	Description	Gene Count	P Value
Biological Process (GO)	GO:0010629	negative regulation of gene expression	12	2.33e-12
Biological Process (GO)	GO:0090304	nucleic acid metabolic process	12	5.05e-08
Biological Process (GO)	GO:0042769	DNA damage response, detection of DNA damage	4	9.62e-08
Biological Process (GO)	GO:0042276	error-prone translesion synthesis	4	2.46e-06
Biological Process (GO)	GO:0006297	nucleotide-excision repair, DNA gap filling	3	3.52e-06
Biological Process (GO)	GO:0070911	global genome nucleotide-excision repair	3	4.76e-06
Biological Process (GO)	GO:0000122	negative regulation of transcription by RNA polymerase II	5	0.00105
KEGG_PATHWAY	hsa03010	Ribosome	11	2.96e-20

Table 1. The top 15 hub genes enrichment with GO and KEGG

5.4 Conclusions

Recently, nanotechnology is emerging as a novel tool with the aim to develop innovative nano-compounds able to sustain the battle against cancer. [40] In the last few years, a large variety of nanomaterials have been investigated for their potential use in oncology, in order to overcome the limitation of current therapies. [41] Several metallic nanoparticles have shown interesting antitumoral activity against human cancer cells. [42] Among them, AgNPs show peculiar physical-chemical features with intrinsic antiproliferative activity. [43, 44] The "green" synthesis approach enables to produce stable AgNPs in an easy and inexpensive way. Following this path, we prepared AgNPs from *Artemisia arborescens* extracts. *Artemisia arborescens* is a plant belonging to the genus *Artemisia,* which contains several compounds, including terpenes and artemisinin with known pharmacological anti-cancer properties. For these reasons, we decided to utilize *Artemisia arborescens* to synthetize AgNPs. *Artemisia*-AgNPs showed a strong cell growth inhibition and G1 cell cycle arrest accompanied by apoptotic induction on cancer cell lines. Bio-organic active agents of *Artemisia arborescens* and Ag^+ ions may work in a synergic way to enhance the anticancer properties of AgNPs. Anyway, further research is needed in order to clarify the effects of *Artemisia*-AgNPs on cancer cells. The transcriptomic analysis showed several up- and down-regulated genes after *Artemisia*-AgNPs treatment. We identified various pathways affected by *Artemisia*-AgNPs, including p53 pathway.

In conclusion, using a combination of functional assays and RNA-Seq, this study revealed that *Artemisia*-AgNPs induced cell apoptosis and inhibited the cell proliferation through cell-cycle arrest, dysregulation of p53 pathway and regulation of gene expression and DNA damage response. We demonstrated the potential anti-cancer activity of *Artemisia*-AgNPs, providing new insights into molecular mechanisms and opening doors for future investigations.

5.5 References

[1] F. Bray, J. Ferlay, I. Soerjomataram, RL. Siegel, L.A. Torre, A. Jemal, *CA Cancer J Clin*., **2018**, 68, 394.

[2] M. Dobbelstein, U. Moll, *Nat. Rev. Drug Discovery*, **2014**, 13, 179.

[3] S. Tran, P. DeGiovanni, B. Piel, P. Rai, *Clin Transl Med*., **2017**, 6, 44.

[4] J. Shi, P.W. Kantoff, R. Wooster, O.C. Farokhzad, *Nature Reviews Cancer*, **2017**, 17, 20.

[5] S.R. Ji, C. Liu, B. Zhang, F. Yang, J. Xu, J. Long, C. Jin, D.L. Fu, Q.X. Ni, X.J. Yu, *Biochim Biophys Acta,* 2010, 1806, 29.

[6] O.L. Gobbo, K. Sjaastad, M.W. Radomski, Y. Volkov, A. Prina-Mello, *Theranostics*, **2015**, 5, 1249.

[7] P.P. Deshpande, S. Biswas, V.P. Torchilin, *Nanomedicine (Lond)*, **2013**, 8, 1509.

[8] K. Sztandera, M. Gorzkiewicz, B. Klajnert-Maculewicz, *Mol Pharm*., **2019**, 16, 1.

[9] P. Grodzinski, M. Silver, L.K. Molnar, *Expert Rev Mol Diagn*., **2006**, 6, 307.

[10] S. Medici, M. Peana, G. Crisponi, V.M. Nurchi, J.I. Lachowicz, M. Remelli, M.A. Zoroddu, *Coordination Chemistry Reviews*, **2016**, 327, 349.

[11] P. Foroozandeh, A.A. Aziz, *Nanoscale Res Lett*., **2018**, 13, 339.

[12] A.A. Dayem, M.K. Hossain, S.B. Lee, K. Kim, S.K. Saha, G.M. Yang, H.Y. Choi, S.G. Cho, *Int J Mol Sci.*, **2017**, 18, 120.

[13] D. Guo, L. Zhu, Z. Huang, H. Zhou, Y. Ge, W. Ma, J. Wu, X. Zhang, X. Zhou, Y. Zhang, Y. Zhao, N. Gu, *Biomaterials*, **2013**, 34, 7884.

[14] S. Ahmed, M. Ahmad, B.L. Swami, S. Ikram, *J Adv Res*., **2016**, 7, 17.

[15] N. Soni, S. Prakash, *American Journal of Nanotechnology*, **2011**, 2, 112.

[16] A. Albanese, P.S. Tang, W.C. Chan, *Annu Rev Biomed Eng*., **2012**, 14:1.

[17] T. Rajabnia, A. Meshkini, *Process Biochem*., **2018**, 65, 186.

[18] A.K. Bhunia, P.K. Samanta, D. Aich, S. Saha, T. Kamilya, *J. Phys. D: Appl. Phys.,* **2015**, 48, 23.

[19] M. Saddi, A. Sanna, F. Cottiglia, L. Chisu, L. Casu, L. Bonsignore, A. De Logu, *Annals of Clinical Microbiology and Antimicrobials,* **2007**, 6, 10.

[20] Y. Alam-Faruque, E. C. Dimmer, R.P. Huntley, C. O'Donovan, P. Scambler and R. Apweiler, *Organogenesis*, **2010**, 6, 71.

[21] M. Kanehisa, *Novartis Found Symp*, **2002**, 247, 91.

[22] K. Urbańska, B. Pająk, A. Orzechowski, J. Sokołowska, M. Grodzik, E. Sawosz, M. Szmidt, P. Sysa, *Nanoscale Res Lett.*, **2015**, 10, 98.

[23] S.A. Loutfy, N.A. Al-Ansary, N.T. Abdel-Ghani, A.R. Hamed, M.B. Mohamed, J.D. Craik, T.A. Eldin, A.M. Abdellah, Y. Hussein, M.T. Hasanin, S.E. Elbehairi, *Asian Pac J Cancer Prev*., **2015**, 16, 6039.

[24] P.V. Asharani, M.P. Hande, S. Valiyaveettil, *BMC Cell Biol*., **2009**, 10, 65.

[25] I. Sur, M. Altunbek, M. Kahraman, M. Culha, *Nanotoxicology*, **2010**, 4, 319.

[26] W. Liu, Y. Wu, C. Wang, H.C. Li, T. Wang, C.Y. Liao, L. Cui, Q.F. Zhou, B. Yan, G.B. Jiang, *Nanotoxicology*, **2010**, 4, 319.

[27] F. Lu, S.H. Wu, Y. Hung, C.Y. Mou, *Small*, **2009**, 5, 1408.

[28] W. Jiang, B.Y.S. Kim, J.T. Rutka, W.C.W. Chan, *Nat. Nanotechnol*., **2008**, 3, 145.

[29] S. Khorrami, A. Zarrabi, M. Khaleghi, M. Danaei, M.R. Mozafari, *Int J Nanomedicine*, **2018**, 13, 8013.

[30] E.S. Al-Sheddi, N.N. Farshori, M.M. Al-Oqail, S.M. Al-Massarani, Q. Saquib, R. Wahab, J. Musarrat, A.A. Al-Khedhairy, M.A. Siddiqui, *Bioinorg Chem Appl.*, **2018**, 2018, 9390784.

[31] Y.S. Lee, D.W. Kim, Y.H. Lee, J.H. Oh, S. Yoon, M.S. Choi, S.K. Lee, J.W. Kim, K. Lee, C.W. Song, *Arch Toxicol*., **2011**, 85, 1529.

[32] P.V. AshaRani, G. Low Kah Mun, M.P. Hande, S.Valiyaveettil, *ACS Nano*, **2009**, 3, 279.

[33] D. Kovács, N. Igaz, C. Keskeny, P. Bélteky, T. Tóth, R. Gáspár, D. Madarász, Z. Rázga, Z. Kónya, I.M. Boros, M. Kiricsi, *Sci Rep*., **2016**, 6, 27902.

[34] P. Gopinath, S.K. Gogoi, A. Chattopadhyay, S.S. Ghosh, Nanotechnology, 2008, 19: 075104.

[35] Y. Hsin, C. Chen, S. Huang, T. Shih, P. Lai, P. Chueh, *Toxicol Lett*, **2008**, 179, 130.

[36] S.R. Satapathy, P. Mohapatra, R. Preet, D. Das, B. Sarkar, T. Choudhuri, M.D Wyatt, C.N. Kundu, *Nanomedicine (Lond),* **2013**, 8, 1307.

[37] H. Çiftçi, M. Türk, U. Tamer, S. Karahan, Y, Menemen, *Turk J Biol*, **2013**, 37, 573.

[38] S. Gurunathan, M. Qasim, C. Park, H. Yoo, J.H. Kim, K. Hong, *Int J Mol Sci*., **2018**, 19, 2269.

[39] S. Gurunathan, J.K. Jeong, J.W. Han, X.F. Zhang, J.H. Park, J.H. Kim, *Nanoscale Res Lett*., **2015**, 10, 35.

[40] C.M Hartshorn, M.S. Bradbury, G.M. Lanza, A.E. Nel, J. Rao, A.Z. Wang, U.B. Wiesner, L. Yang, P. Grodzinski, *ACS nano*, **2018**, 12, 24.

[41] E. Hong, M.A. Dobrovolskaia, *Adv Drug Deliv Rev*, **2018**, 141, 3.

[42] P.B. da Silva, R.T.A. Machado, A.M. Pironi, R.C. Alves, P.R. de Araújo, A.C. Dragalzew, I. Dalberto, M. Chorilli, *Curr Med Chem*, **2019**, 26, 2108.

[43] P.V. Asharani, M.P. Hande, S. Valiyaveettil, *BMC Cell Biol*., **2009**, 10, 65.

[44] M.J. Ahmed, G. Murtaza, F. Rashid and J. Iqbal, *Drug Dev Ind Pharm*, **2019**, 45, 1682.

6. Conclusions and future perspective

The experimental evidences herein provided demonstrate the potential applications of nanotechnology in bone regeneration and cancer therapy. Above all, the design of nanomaterials is crucial for the development of advanced tools for specific medical uses. This thesis focused the attention on two innovative nano-compounds: graphene conjugated with calcium phosphate (maGO-CaP) and silver nanoparticles synthesized using *Artemisia arborescence* (*Artemisia*-AgNPs).

Firstly, herein the main characteristics of graphene and its derivates are described, illustrating their perspective use to sustain bone regeneration. Using several functional assays, we demonstrated how maGO-CaP promoted osteogenesis stimulating hMSCs differentiation. The *in vivo* results revealed the biocompatibility of maGO-CaP and its osteoblast-promoting effects, confirming its promising action on bone formation. These results pave the way for further investigation and the development of new strategies to fight bone-related disorders.

On the other hand, the *Artemisia*-AgNPs have been taken into account for their interesting outcomes in cancer research. The cancer nanomedicine research area is emerging in the last few years with interesting outcomes. The antiproliferative activity and apoptotic effects of *Artemisia*-AgNPs on cell cancer lines were evaluated with several approaches. The RNA-sequencing analysis allowed to observe in depth the molecular mechanism involved in the anti-cancer action of *Artemisia*-AgNPs. Anyway, additional considerations are needed to clarify the biological effects of *Artemisia*-AgNPs in order to offer real opportunities in cancer therapy.

To conclude, this thesis proposes new insights for the development of innovative nanoscale platforms, helping to achieve the hoped medical revolution of nanomedicine. The nanomedicine applications need to consider the multidisciplinary nature of this research area to achieve positive results, intensifying the collaborations on several fronts. The involvement of scientists with various backgrounds is of paramount importance, including biologists, chemists, clinicians, and engineers. It is expected that future studies will continue to investigate safe nano-compounds toward personalized medicine, considering the physiological and pathophysiological variability between patients.